

PRECISION STELLAR CHARACTERIZATION OF FGKM STARS USING AN EMPIRICAL SPECTRAL LIBRARY

SAMUEL W. YEE^{1,2}, ERIK A. PETIGURA^{1,3}, AND KASPAR VON BRAUN⁴

¹California Institute of Technology

²syee@caltech.edu

³Hubble Fellow

⁴Lowell Observatory, 1400 W. Mars Hill Rd., Flagstaff, AZ 86001

ABSTRACT

Classification of stars, by comparing their optical spectra to a few dozen spectral standards, has been a workhorse of observational astronomy for more than a century. Here, we extend this technique by compiling a library of optical spectra of 404 touchstone stars observed with Keck/HIRES by the California Planet Search. The spectra are high-resolution ($R \approx 60000$), high signal-to-noise (SNR $\approx 150/\text{pixel}$), and registered onto a common wavelength scale. The library stars have properties derived from interferometry, asteroseismology, LTE spectral synthesis, and spectrophotometry. To address a lack of well-characterized late K-dwarfs in the literature, we measure stellar radii and temperatures for 23 nearby K-dwarfs, using SED modeling and *Gaia* parallaxes. This library represents a uniform dataset spanning the spectral types $\sim M5$ – $F1$ ($T_{\text{eff}} \approx 3000$ – 7000 K, $R_{\star} \approx 0.1$ – $16 R_{\odot}$). We also present “Empirical SpecMatch” (**SpecMatch-Emp**), a tool for parameterizing unknown spectra by comparing them against our spectral library. For FGKM stars, **SpecMatch-Emp** achieves accuracies of 100 K in effective temperature (T_{eff}), 15% in stellar radius (R_{\star}), and 0.09 dex in metallicity ($[\text{Fe}/\text{H}]$). Because the code relies on empirical spectra it performs particularly well for stars $\sim K4$ and later which are challenging to model with existing spectral synthesizers, reaching accuracies of 70 K in T_{eff} , 10% in R_{\star} , and 0.12 dex in $[\text{Fe}/\text{H}]$. We also validate the performance of **SpecMatch-Emp**, finding it to be robust at lower spectral resolution and SNR, enabling the characterization of faint late-type stars. Both the library and stellar characterization code are publicly available.

1. INTRODUCTION

Measuring the physical properties of stars is a long-standing and important problem in astronomy. The masses, radii, and temperatures of stars are benchmarks against which we test models of stellar structure and evolution. The abundances of iron and other elements in stellar populations help trace the nucleosynthetic enrichment history of the Milky Way. Recently, the study of extrasolar planets has placed new demands on *precision* stellar characterization. The extent to which observational methods like radial velocities and transit photometry can reveal a planet’s mass and radius is limited by the uncertainty in stellar mass and radius, respectively.

Eclipsing binaries typically offer the most precise and least model-dependent measurements of stellar mass (M_{\star}) and radius (R_{\star}), relying primarily on Newtonian mechanics and geometry. Analysis of eclipsing binary light curves and radial velocities can achieve measurements of M_{\star} and R_{\star} good to $\lesssim 3\%$. After incorporating broadband photometry and parallaxes, eclipsing bina-

ries can yield effective temperatures (T_{eff}) good to $\sim 2\%$ (Torres et al. 2010).

Measurements of such stellar properties for isolated field stars are more challenging and rely more heavily on models of stellar interiors and atmospheres. Recently, precision space-based photometry from the *Kepler* and *CoRoT* missions (Borucki et al. 2010; Auvergne et al. 2009) have enabled the detection of stellar acoustic modes which achieve M_{\star} and R_{\star} good to a few % (e.g. Bruntt et al. 2012, Huber et al. 2013). The amplitude of these modes grows with the size of the star and have been detected in stars that are roughly solar-size or larger. For smaller stars, the acoustic oscillation amplitudes are smaller, making their detection increasingly difficult against photometric noise due to photon Poisson statistics, surface granulation, and other sources of stellar activity. While asteroseismology has provided some excellent stellar benchmarks, it is not applicable for all stellar types. This illustrates a recurring challenge in the field of precision stellar astrophysics: no single technique is uniformly effective across the Hertzsprung-

Russell (HR) diagram.

Recently, optical and infrared interferometry have been used to directly measure the angular size of stars (e.g. von Braun et al. 2014). When combined with parallax measurements and an observed spectral energy distribution, this technique provides T_{eff} and R_{\star} that are almost purely empirical. Interferometry requires stars that are nearby and bright and thus currently applicable to only a limited number. As of 2016, only about ~ 100 main sequence stars and ~ 200 giants have precision interferometric measurements. Stars cooler than ~ 5000 K are underrepresented in this interferometric sample due to their faintness. Finally, obtaining M_{\star} relies on a spectroscopic measurement of $\log g$ coupled with the directly determined R_{\star} or by using stellar structure models with T_{eff} , R_{\star} , and spectroscopic measurements of the star’s metallicity as input.

Another common technique for stellar characterization relies on detailed modeling of a star’s spectrum. This involves constructing a model stellar atmosphere and modeling the radiative transfer of photons as they emerge from the photosphere on their way toward Earth. The effective temperature, surface gravity ($\log g$), metallicity ($[\text{Fe}/\text{H}]$), abundance of other species, and projected rotational velocity ($v \sin i$) are adjusted until the simulated distribution of photons matches the observed spectrum. Two commonly-used spectral synthesis codes are MOOG (Snedden 1973) and SME (Valenti & Piskunov 1996; Valenti & Fischer 2005; Brewer et al. 2015). One challenge facing spectral synthesis is that model stellar atmospheres grow more uncertain as they diverge from solar. Consequently, such codes may accurately reproduce the observed stellar spectrum, but do so with parameters that may be different from the true stellar properties. Spectral synthesis techniques begin to suffer dramatically for stars having spectral type K4 and later ($T_{\text{eff}} \lesssim 4700$ K), due to the large number of atomic and molecular lines combined with missing or inaccurate values in the input line lists and associated quantum mechanical properties.

With this background in mind, we present a new method, “Empirical SpecMatch” (**SpecMatch-Emp**), for precision stellar characterization based on the direct comparison of observed optical spectra to a dense library of touchstone stars with well-measured properties. A chief goal of **SpecMatch-Emp** is accuracy across the HR diagram with a specific focus on stars of mid-K spectral type and later, due to the uncertainties with associated with synthetic spectral techniques.

SpecMatch-Emp builds off a long history of stellar classification in astronomy using optical spectra. Founding work took place at the Harvard College Observatory (c. 1885–1925) with the visionary and heroic efforts of A. J. Cannon, A. P. Draper, and E. C. Pickering which

culminated in the HD catalog and the OBAFGKM classification sequence. A significant refinement by Morgan et al. (1943) included luminosity classes as a essential second dimension in the sequence (Gray & Corbally 2009).

SpecMatch-Emp extends this methodology by considering a third dimension, metallicity, and by returning numerical measurements of T_{eff} , R_{\star} , and $[\text{Fe}/\text{H}]$ of stellar parameters as opposed to categorical spectral classifications. This approach is enabled by the large and homogeneous sample of high resolution, high signal-to-noise spectra gathered by the California Planet Search as part of its radial velocity programs to study extra-solar planets and by recent work to compile catalogs of touchstone stars with well-measured properties.

SpecMatch-Emp consists of two major parts: a spectral library and an algorithm for parameter measurement. In Section 2, we describe the construction of the spectral library of stars having properties determined by asteroseismology, interferometry, spectroscopy, and spectrophotometry. To address the scarcity of suitable mid- to late-K dwarfs from the literature, we present new precision measurements of 23 K-dwarfs incorporating spectroscopy, SED modeling, and parallax measurements. This library of spectra and stellar parameters are publicly available for download as a monolithic memory-efficient Hierarchical Data Format (HDF5) file¹ or as individual Flexible Image Transport System (FITS) files for each spectrum.²

In Section 3, we describe the **SpecMatch-Emp** algorithm, which compares an unlabelled target spectrum with the spectral library. The code, as well as easy-to-use command-line scripts, can also be obtained online.³ In Section 4, we assess the accuracy of **SpecMatch-Emp** by performing an internal cross-validation analysis. We verified that for stars ranging from $T_{\text{eff}} \approx 3000$ –7000 K, **SpecMatch-Emp** yields T_{eff} , R_{\star} , and $[\text{Fe}/\text{H}]$ good to 100 K, 15%, and 0.09 dex respectively. We also investigate the performance of the algorithm at decreased SNR and spectral resolution by degrading the target spectra. We find that **SpecMatch-Emp** remains robust even at SNR as low as 10/pixel, as well as spectral resolutions down to about $R = 20000$.

2. LIBRARY

A crucial component of the **SpecMatch-Emp** is the spectral library of 404 stars, each with well-determined stellar parameters (M_{\star} , R_{\star} , T_{eff} , $[\text{Fe}/\text{H}]$). As no single

¹ <https://zenodo.org/record/168084/files/library.h5>

² http://web.gps.caltech.edu/~syee/hires_spectra/

³ <https://github.com/samuelyeew1/specmatch-emp>

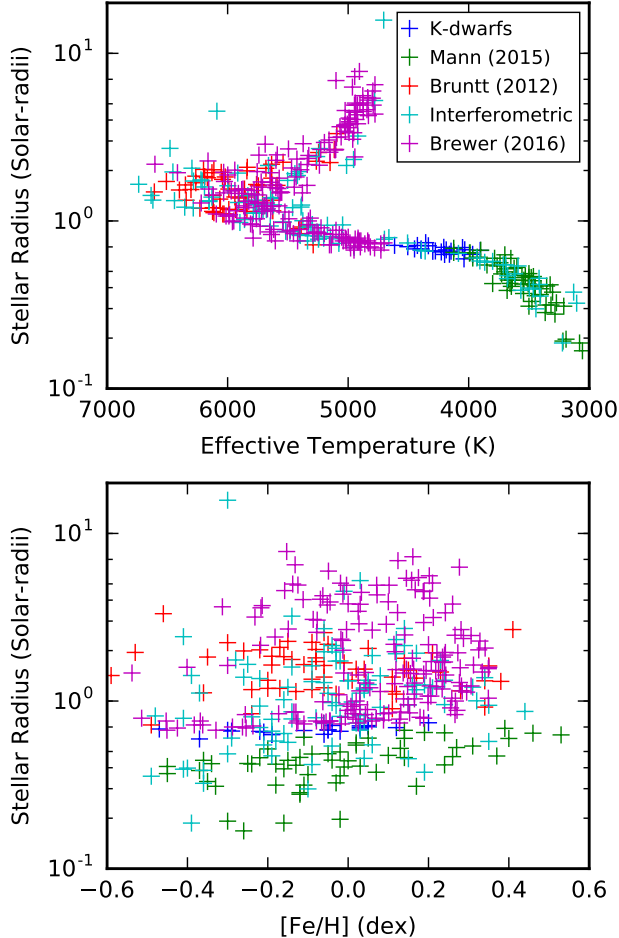


Figure 1. Distribution of SpecMatch-Empirical library stars. The library covers the parameter space of $T_{\text{eff}} \approx 3000 - 7000$ K, $R_{\star} \approx 0.16 - 16 R_{\odot}$, $[\text{Fe}/\text{H}] \approx -0.5 - +0.5$ dex. We have excluded stars having measured $v \sin i > 8.0$ km s $^{-1}$ as their spectra retain insufficient information for the matching process.

technique yields the best parameters across the HR diagram, we have compiled the parameters for the stars in our library from a variety of different sources. By construction, our library contains stars that span a large region of the HR diagram ($T_{\text{eff}} \approx 3000 - 7000$ K, $R_{\star} \approx 0.1 - 16 R_{\odot}$). The domain of T_{eff} , R_{\star} , and $[\text{Fe}/\text{H}]$ is shown in Figure 1 along with the provenance of the library parameters. We describe in brief the source catalogs for these parameters in Section 2.1. We augment this sample with new K-dwarf library stars in Section 2.2. In Section 2.3, we describe our conversion of the measured stellar properties into a homogeneous suite of T_{eff} , $\log g$, $[\text{Fe}/\text{H}]$, M_{\star} , R_{\star} , and age measurements for each star. The details of the spectral dataset are described in Section 2.4.

2.1. Library Parameters

2.1.1. Interferometric sample

The library includes 95 stars having interferometrically-determined radii with quoted uncertainties in radius of $< 5\%$ compiled by von Braun et al. (2014).⁴ This set of interferometric stars is the only sample included in our library to span the entire HR diagram, as the other techniques face limitations in different regions of the parameter space. However, the relatively small number of stars with interferometric measurements necessitated the inclusion of stars from other sources.

2.1.2. Mann et al. 2015

Mann et al. (2015) measured fundamental properties of 183 late K and M dwarfs by performing an absolute flux calibration on optical and NIR spectra using literature photometry. The photometric measurements were calibrated with the updated filter profiles from Mann & von Braun (2015). The bolometric flux (F_{bol}) was calculated by integrating over the flux-calibrated spectra, while T_{eff} was obtained by comparing the spectra with PHOENIX stellar atmosphere models. F_{bol} and T_{eff} were then combined distance, d , measured by trigonometric parallax, to obtain the physical radius of the star (R_{\star}) using the Stefan-Boltzmann law,

$$L_{\star} = 4\pi d^2 F_{\text{bol}} = 4\pi R_{\star}^2 \sigma T_{\text{eff}}^4.$$

The analysis used empirical relations between spectral feature widths and $[\text{Fe}/\text{H}]$ from Mann et al. (2013) and Mann et al. (2014) to obtain the stellar metallicities. M_{\star} was determined using empirical mass-luminosity relations from Delfosse et al. (2000). Both of these empirical relationships have been calibrated for M dwarfs. Median uncertainties for the stellar properties were 60 K in T_{eff} , 3.8% in R_{\star} , 0.08 dex in $[\text{Fe}/\text{H}]$ and 10% in M_{\star} . Our library includes 56 of the stars from this sample, for which we had suitable HIRES spectra. These comprise the majority of the M dwarfs in our library.

2.1.3. Brewer et al. 2016

Brewer et al. (2016) conducted a detailed spectroscopic analysis of 1617 dwarf and subgiant stars with $T_{\text{eff}} = 4700 - 6800$ K observed by Keck/HIRES. Brewer et al. (2016) modeled the spectra with SME (Valenti & Piskunov 1996) which has been recently updated to include many more lines (Brewer et al. 2015). We chose 177 of the stars from this analysis for our library, excluding stars with $v \sin i > 8$ km s $^{-1}$, $\text{SNR} < 120$ per pixel, and $[\text{Fe}/\text{H}] < -1.0$ dex. We adopted the following uncertainties for the stellar parameters: 60 K in T_{eff} , 0.05

⁴ The von Braun et al. (2014) compilation included results from Kervella et al. (2003), Baines et al. (2008), Baines et al. (2009), van Belle & von Braun (2009), von Braun et al. (2011a), von Braun et al. (2011b), von Braun et al. (2012), Boyajian et al. (2013), and Henry et al. (2013).

dex in $\log g$, and 0.05 dex in $[\text{Fe}/\text{H}]$ based on the comparisons with other independent techniques performed in [Brewer et al. \(2015\)](#) and [Brewer et al. \(2016\)](#).

2.1.4. *Bruntt et al. 2012*

[Bruntt et al. \(2012\)](#) examined 93 solar-type stars observed by *Kepler*, combining asteroseismology and spectroscopy to measure T_{eff} , $\log g$, and $[\text{Fe}/\text{H}]$. The quoted uncertainties on these properties were 0.03 dex in $\log g$, 60 K in T_{eff} , and 0.06 dex in $[\text{Fe}/\text{H}]$. We included 55 stars from this sample with HRES spectra in our library.

2.2. *K Dwarfs*

Finding well-characterized mid to late K-dwarfs (K4–K7; $T_{\text{eff}} \approx 4700\text{--}4000$ K) proved to be particularly challenging. Detailed spectral synthesis codes such as *SME* and *MOOG* are challenged by the proliferation of deep metallic lines and the onset of MgH and TiO bands ([Gray & Corbally 2009](#)). The empirical relations used in [Mann et al. \(2015\)](#) have not been calibrated for spectral types earlier than K7 ($T_{\text{eff}} \lesssim 4100$ K). While measurements based on CHARA interferometry exist for a few such stars, coverage is sparse due to the small number of stars that are both bright enough at optical wavelengths and close enough for precise radius measurements.

Due to the paucity of touchstone stars in the literature, we derived T_{eff} and R_{\star} for 23 K4–K7 dwarfs using broadband photometry and constraints from parallax, π_{\star} . We drew stars from a sample of 110 included in a survey of planets around late K-dwarfs ([Gaidos et al. 2013](#)). After a search of literature photometry, we restricted this sample to the 23 stars having at least one literature measurement in the *UBVRIJHK* bands, which provide good coverage across the stellar Spectral Energy Distribution (SED).

We derived T_{eff} using an empirical $V - K$ color-temperature relationship from [Boyajian et al. \(2013\)](#)

$$T_{\text{eff}} = a_0 + a_1(V - K) + a_2(V - K)^2 + a_3(V - K)^3$$

where

$$\begin{aligned} a_0 &= 8649 \pm 28 \text{ K} \\ a_1 &= -2503 \pm 35 \text{ K mag}^{-1} \\ a_2 &= 442 \pm 12 \text{ K mag}^{-2} \\ a_3 &= -31.7 \pm 1.5 \text{ K mag}^{-3} \end{aligned}$$

The coefficients a_i are found in Table 8 of [Boyajian et al.](#)

(2013) and were calibrated to 125 FGK stars with literature photometry and effective temperatures. Using this relation with existing literature photometry for our sample of K dwarfs, we were able to find T_{eff} to a typical uncertainty of $\sim 5\%$.

Next, we measured F_{bol} by fitting the broadband photometry with a stellar SED and integrating over wavelength. Our procedure for the SED fitting follows [von Braun et al. \(2014\)](#): we used the library of spectral templates from [Pickles \(1998\)](#) and fit them to literature photometry data via χ^2 -minimization. We linearly interpolated between the published spectral templates to the nearest half spectral type to improve χ^2 fitting. For the literature photometry data, we make use of the modified filter profiles from [Mann & von Braun \(2015\)](#). Reddening is set to zero for all targets due to their small distances (< 26 pc). After the template is scaled to minimize the reduced χ^2 , bolometric flux is measured by integrating over wavelength.

Twenty one stars from our sample have updated parallaxes from new Gaia data, as part of the Tycho-Gaia Astrometric Solution (TGAS; [Gaia Collaboration et al. 2016](#); [Lindgren et al. 2016](#); [Michalik et al. 2015](#)). These stars have uncertainties in parallax, $\sigma(\pi_{\star}) \approx 0.3$ mas. For the remaining two stars (GJ 1172 and HD 85488), we used the parallax values calculated in the van Leeuwen reduction of *Hipparcos* data with $\sigma(\pi_{\star}) \approx 1.6$ mas ([Perryman et al. 1997](#); [van Leeuwen 2007](#)). Combining T_{eff} , F_{bol} , π_{\star} and the Stefan-Boltzmann law, we calculated R_{\star} . The median uncertainty in R_{\star} over the entire sample was 7.4%, dominated primarily by the uncertainties in T_{eff} from the color-temperature relation.

Finally, we adopted the metallicity values found in [Gaidos et al. \(2013\)](#), which were derived using *SME* ([Valenti & Piskunov 1996](#)). While traditional spectroscopic techniques begin to suffer for $T_{\text{eff}} \lesssim 4700$ K, they are the only source of metallicity measurements for this sample of K dwarfs. More accurate metallicities could be derived by observing K-dwarfs with G-dwarf companions for which metallicity can be measured more accurately from spectral synthesis. Such a study is beyond the scope of this work. We adopt 0.1 dex as the uncertainty on $[\text{Fe}/\text{H}]$ and note that such errors are likely systematic (rather than statistical) in nature. The final set of parameters used for these K dwarfs are listed in Table 1.

Table 1. Properties of 23 K-Dwarfs

Name	HIP	V mag	K mag	T_{eff} K	F_{bol} $10^{-8} \text{erg}^{-1} \text{cm}^{-2}$	π_* mas	R_* R_{\odot}	[Fe/H] dex	Notes
GJ 1008.0	1532	9.92 ± 0.04	6.58 ± 0.03	4039 ± 241	0.66 ± 0.01	49.3 ± 0.4	0.59 ± 0.06	-0.37 ± 0.10	1
GJ 1044	10337	9.86 ± 0.04	6.54 ± 0.03	4051 ± 239	0.68 ± 0.01	42.6 ± 0.9	0.69 ± 0.07	0.12 ± 0.10	1
GJ 1127	47201	9.45 ± 0.03	6.37 ± 0.03	4207 ± 212	0.86 ± 0.01	44.5 ± 0.2	0.70 ± 0.05	0.03 ± 0.10	1
GJ 1172	66222	9.95 ± 0.04	6.38 ± 0.03	3904 ± 266	0.71 ± 0.01	48.8 ± 1.6	0.67 ± 0.09	-0.11 ± 0.10	2
GJ 3072	4845	10.03 ± 0.04	6.57 ± 0.06	3967 ± 301	0.62 ± 0.01	46.7 ± 0.4	0.63 ± 0.07	-0.19 ± 0.10	1
GJ 3494	40910	9.76 ± 0.04	6.61 ± 0.03	4159 ± 228	0.68 ± 0.01	44.3 ± 0.3	0.63 ± 0.05	-0.06 ± 0.10	1
GJ 9093	12493	9.52 ± 0.03	6.54 ± 0.03	4276 ± 193	0.74 ± 0.01	41.9 ± 0.3	0.66 ± 0.05	-0.29 ± 0.10	1
GJ 9144	19165	9.69 ± 0.03	6.74 ± 0.03	4298 ± 200	0.64 ± 0.01	38.7 ± 0.2	0.66 ± 0.05	-0.22 ± 0.10	1
HD 178126	93871	9.22 ± 0.02	6.47 ± 0.03	4449 ± 177	0.87 ± 0.01	40.8 ± 0.3	0.68 ± 0.04	-0.47 ± 0.10	1
HD 200779	104092	8.30 ± 0.02	5.33 ± 0.04	4283 ± 211	2.47 ± 0.01	66.6 ± 0.2	0.76 ± 0.06	0.07 ± 0.10	1
HD 20280	15095	9.16 ± 0.02	6.11 ± 0.03	4227 ± 199	1.14 ± 0.01	54.0 ± 0.3	0.65 ± 0.05	-0.21 ± 0.10	1
HD 203040	105341	9.10 ± 0.04	5.75 ± 0.03	4033 ± 242	1.38 ± 0.01	63.2 ± 0.5	0.67 ± 0.06	-0.05 ± 0.10	1
HD 218294	114156	9.62 ± 0.02	6.45 ± 0.03	4146 ± 209	0.75 ± 0.01	45.1 ± 0.3	0.66 ± 0.05	-0.02 ± 0.10	1
HD 224607	118261	8.70 ± 0.05	6.15 ± 0.03	4615 ± 214	1.29 ± 0.01	44.0 ± 0.2	0.71 ± 0.05	-0.04 ± 0.10	1
HD 35171	25220	7.94 ± 0.03	5.26 ± 0.03	4505 ± 179	2.74 ± 0.02	68.5 ± 0.3	0.70 ± 0.04	0.05 ± 0.10	1
HD 355784	97051	9.96 ± 0.05	6.87 ± 0.03	4200 ± 248	0.53 ± 0.01	38.5 ± 0.3	0.63 ± 0.06	-0.19 ± 0.10	1
HD 59582	36551	8.98 ± 0.03	6.16 ± 0.03	4395 ± 193	1.13 ± 0.01	48.5 ± 0.3	0.67 ± 0.05	-0.30 ± 0.10	1
HD 68834	40375	8.82 ± 0.04	5.92 ± 0.03	4334 ± 209	1.39 ± 0.01	52.0 ± 0.3	0.71 ± 0.05	0.03 ± 0.10	1
HD 7279	5663	9.56 ± 0.04	6.45 ± 0.03	4186 ± 222	0.77 ± 0.01	44.0 ± 0.3	0.67 ± 0.06	-0.05 ± 0.10	1
HD 80632	45839	9.10 ± 0.04	6.32 ± 0.03	4426 ± 198	0.99 ± 0.01	41.8 ± 0.2	0.71 ± 0.05	0.05 ± 0.10	1
HD 85488	48411	8.85 ± 0.03	5.98 ± 0.03	4357 ± 199	1.30 ± 0.01	47.7 ± 1.5	0.74 ± 0.07	0.20 ± 0.10	2
HD 97214	54651	9.23 ± 0.03	6.36 ± 0.03	4357 ± 197	0.87 ± 0.01	50.5 ± 0.4	0.58 ± 0.04	-0.89 ± 0.10	1
HD 97503	54810	8.70 ± 0.02	5.88 ± 0.03	4395 ± 185	1.46 ± 0.01	54.2 ± 0.3	0.68 ± 0.04	0.03 ± 0.10	1

NOTE—Parameters of newly-characterized K4-K7 dwarfs determined by combining an empirical color-temperature relation, SED-fitting, and stellar parallaxes.

¹ Parallax from the Tycho-Gaia Astrometric Solution (TGAS; [Gaia Collaboration et al. 2016](#); [Lindgren et al. 2016](#); [Michalik et al. 2015](#)).

² Parallax from Hipparcos.

2.3. Isochrone Analysis

The catalogs of stars presented in Section 2.1 often do not list a complete set of T_{eff} , R_* , M_* , $\log g$, and [Fe/H]. For example, the interferometric sample (Section 2.1.1) does not include measurements of M_* . To obtain a homogeneous suite of parameters, we combine the known properties with the Dartmouth models ([Dotter et al. 2008](#)). We use the `isochrones` software package ([Mor-ton 2015](#)), which performs an MCMC fit to estimate the remaining stellar parameters from the stellar model grid. To account for systematic errors in the Dartmouth models, we adopt the 5th and 95th percentiles of the final MCMC distribution as the parameter uncertainties.

2.4. Optical Spectra

The spectra were observed with the High Resolution Echelle Spectrometer (HIRES; [Vogt et al. 1994](#)) at the Keck-I 10-m telescope as part of the various programs by the California Planet Search to study extrasolar planets.

For information about CPS and its goals, see [Howard et al. \(2010\)](#). The spectra have a resolution, $R \approx 50000$ – 60000 . We selected stars with spectra having SNR of at least 40 per pixel, with most ($\sim 80\%$) having signal-to-noise ratio (SNR) of >100 per HIRES pixel on blaze near 550 nm.

The extracted spectra are from the middle chip of HIRES and contain 16 orders with 4021 intensity measurements per order. Each order is imprinted with the HIRES blaze function which we remove by dividing the observed spectrum with a calibration spectrum constructed from several rapidly rotating B-stars. Due to different line of sight velocities, the library spectra are shifted with respect to one another in pixel-coordinates. It is convenient to adopt a common wavelength scale and register each spectrum to this scale. We resampled our spectra onto a new wavelength scale ($\lambda = 4990$ – 6410 \AA) that is uniform in $\Delta \log \lambda$. We then removed the shifts due to the stars’ individual line of sight veloci-

ties by registering our spectra against the National Solar Observatory (NSO) solar spectrum (Kurucz et al. 1984) according to the procedure described in Section 3.1. The final library data set thus consists of a 404×73788 array of normalized spectra on the rest wavelength scale, together with associated stellar parameters.

3. SPECMATCH

Here, we describe the `SpecMatch-Emp` algorithm. Given an unknown spectrum, `SpecMatch-Emp` first shifts it onto the library wavelength scale to correct for their individual radial velocity (Section 3.1). We then identify the most similar library spectra (Section 3.2) and interpolate between them (Section 3.3) to arrive at a final set of derived parameters for the target star.

We report T_{eff} , R_{\star} , and $[\text{Fe}/\text{H}]$ in contrast to most spectral analysis codes, which report T_{eff} , $\log g$, and $[\text{Fe}/\text{H}]$. While R_{\star} is closely related to $\log g$, for the library stars K4 and later, R_{\star} is the directly observed quantity. We could, in principle, derive $\log g$ values by appealing to stellar models, but such models have known systematic errors that are largest for cool stars. For example, in their study of M-dwarfs, Mann et al. (2015) found that the Dartmouth models systematically over-predict stellar radii by $\approx 5\%$. Therefore, to mitigate systematic errors in the derived stellar radii of late-type stars, where `SpecMatch-Emp` performs best, we choose to parametrize stars in terms of T_{eff} , R_{\star} , and $[\text{Fe}/\text{H}]$.

3.1. Spectral Registration

We begin by resampling each of the 16 orders of the HIRES spectrum onto the library wavelength scale. Because the library wavelength scale is uniform in $\Delta \log \lambda$, fixed velocity shifts between the spectra correspond a uniform displacement in the current logarithmic wavelength sampling. We also mask out the telluric lines due to atmospheric O_2 absorption in the $\lambda = 6270 - 6310 \text{ \AA}$ wavelength region, as these lines are fixed in the observatory frame, not in the stellar rest frame.

Each masked order is then divided into segments of length ~ 700 pixels, which are then cross-correlated with the reference spectrum. This operation is performed in Fourier space and low frequency Fourier modes are filtered out such that only spectral lines, and not long-baseline differences in continuum normalization, contribute to the cross-correlation. For each segment, we find the ideal pixel shift by fitting a parabola to the cross-correlation peak. We fit a line through these shifts to obtain a linear relationship between the pixel shift and pixel number across each order (Figure 2). As an example, we show the observed and registered spectrum of HD190406 in Figure 3.

As a matter of convenience, all the library spectra are shifted onto a single wavelength scale, chosen to

be that of the NSO solar spectrum. However, for stars with spectral types unlike the Sun, performing the cross-correlation against the NSO spectrum gives poor results, with multiple spurious peaks which do not correspond to the true velocity shift (see top panel of Figure 4).

To address this, we use a bootstrapping approach in which four additional spectra belonging to stars of different spectral types were shifted successively onto the NSO wavelength scale, forming a ladder of template spectra. These additional spectra were chosen from our highest signal-to-noise spectra ($\text{SNR} > 160/\text{pixel}$), with roughly solar metallicities and spaced evenly in T_{eff} and R_{\star} . When presented with an unknown target spectrum, we find the best reference spectrum by performing the cross-correlation procedure described above on a single order of the target spectrum. The reference spectrum which gives the largest median cross-correlation peak with the target is deemed to have the greatest similarity to the target and is then used to shift the rest of the target spectrum. We selected the spectral order that spans $\lambda = 5120 - 5210 \text{ \AA}$ as the benchmark order due to the rich spectral information contained in this region across all spectral types. In Figure 5, we illustrate the successful registration of Barnard’s star (GL699, spectral type M4V) to the NSO scale with our bootstrapping approach.

3.2. Matching

Once the target spectrum has been shifted and flattened onto the library wavelength scale, we compare it to each of the library spectra, in segments of 100 \AA (see table 2). In each comparison, we first modify the library spectrum by applying a rotational broadening kernel (Equation 17.12 in Gray 1992) to account for the relative $v \sin i$ between the target and reference stars. We found that it was necessary to set a maximum relative $v \sin i$ limit, chosen to be 10 km s^{-1} , to prevent the reference spectrum from being broadened excessively. If the kernel was allowed to go to arbitrarily high $v \sin i$ values, it would allow seemingly better matches even with dissimilar spectra due to the loss of spectral information from broadening. We also fit a cubic spline through the residuals between the target and reference spectra, using knots placed at 20 \AA intervals. Subtracting out this spline amounts to a high-pass filter which ensures that the χ^2 is not influenced by slowly-varying ($\gtrsim 20 \text{ \AA}$) residual structure due to imperfections in the blaze function removal.

We adopt the unnormalized χ^2 statistic the figure of merit that quantifies degree of similarity between the target and modified reference spectra:

$$\chi^2 = \sum (s_{\text{ref}} - s_{\text{target}})^2.$$

The pixel-by-pixel Poisson uncertainties are not in-

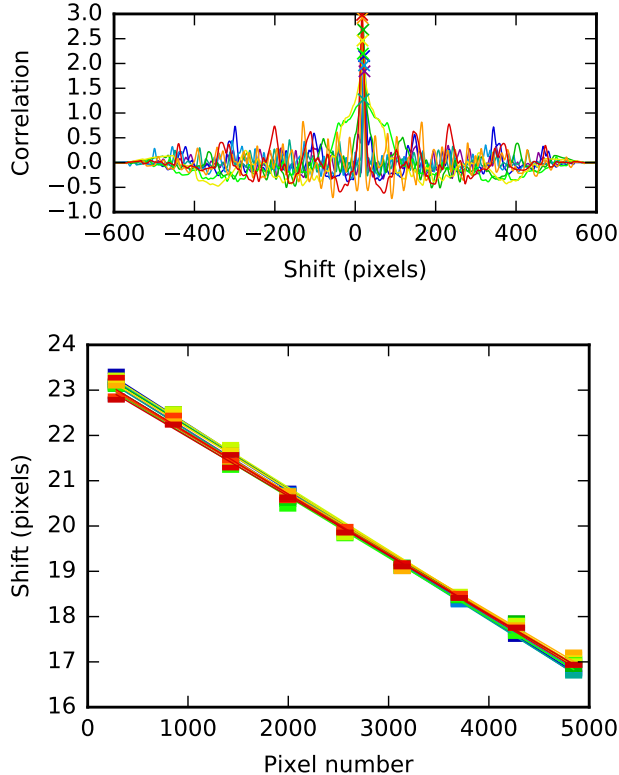


Figure 2. Registration of a solar-type spectrum using cross-correlation (see § 3.1). Top: Cross-correlation of a single order of the spectrum of HD190406 (spectral type G0V) with corresponding regions of the solar spectrum. Each line corresponds to a particular segment. The maximum correlation for each segment is indicated with a cross. Bottom: The shifts calculated for the various segments of each order are fit with a first order polynomial, which is then applied to shift the corresponding pixels. Outliers result from poor cross-correlation results in that region of spectrum and are clipped before the fit is performed.

cluded because the main residual differences in the spectra are due to astrophysical differences, not photon noise. Including photon errors would give lower χ^2 values when comparing with library spectra with poorer signal-to-noise ratios, even if these spectra are dissimilar to the target. We verify in Section 4.2 that **SpecMatch-Emp** is dominated by systematics, not photon statistics down to SNR of 10/pixel.

Allowing for $v \sin i$ and continuum normalization to float as free parameters, we use a non-linear least-squares minimization package `lmfit` (Newville et al. 2014) to minimize χ^2 , finding the best possible match between the target and reference spectra. We then repeat this matching process over all the library spectra, recording in each case the lowest χ^2 value achieved. We illustrate the results of the matching step for a HD190406, a solar-type star, and Barnard’s star (GL699), an M4V star in Figures 6 and 7. Figure 6 shows the best-matching spectra from the library and

Figure 7 shows the distribution of χ^2 .

Region	Wavelength Range
1	5000 – 5100 Å
2	5100 – 5200 Å
3	5200 – 5300 Å
4	5300 – 5400 Å
5	5400 – 5500 Å
6	5500 – 5600 Å
7	5600 – 5700 Å
8	5700 – 5800 Å

Table 2. Wavelength regions used in both the matching and linear combination steps in **SpecMatch-Emp**.

3.3. Linear Combination

The **SpecMatch-Emp** routine then interpolates between the parameters of the library spectra by synthesizing linear combinations of the five best-matching spectra as found in the previous step. We form a new composite spectrum, $S_{lc} = \sum_{i=1}^5 c_i \cdot S_i$, where each spectrum, S_i , is broadened by the optimal $v \sin i$ found in the previous matching stage. We chose to use five spectra in these linear combinations by trial and error. We use `lmfit` to find the set of coefficients $\{c_1, c_2, \dots, c_5\}$ which minimizes χ^2 when compared with the target spectrum. The c_i ’s are subject to the constraint that they should sum to unity by incorporating a narrow Gaussian prior of width $\sigma = 10^{-3}$, such that χ^2 :

$$\chi^2 = \sum (s_{lc} - s_{target})^2 + \left(\sum c_i - 1 \right)^2 / 2\sigma^2.$$

In this step, we continue to correct for differences in continuum normalization by fitting a cubic spline and allowing the spline parameters to float as we minimize χ^2 .

We thus obtain a new spectrum which matches the target spectrum even more closely than any individual library spectrum. We show example results in Figures 8 and 9.

The set of coefficients c_i found which minimizes χ^2 is then used to create a weighted average of the parameters of the reference stars. In order to incorporate the spectral information from the entire spectrum, we average the derived parameters from each 100 Å segment to obtain a final set of stellar parameters for the target. In total, it takes approximately 10 minutes to obtain the final parameters from a raw, unshifted spectrum on a modern (c. 2016) desktop computer.

4. PERFORMANCE

4.1. Accuracy

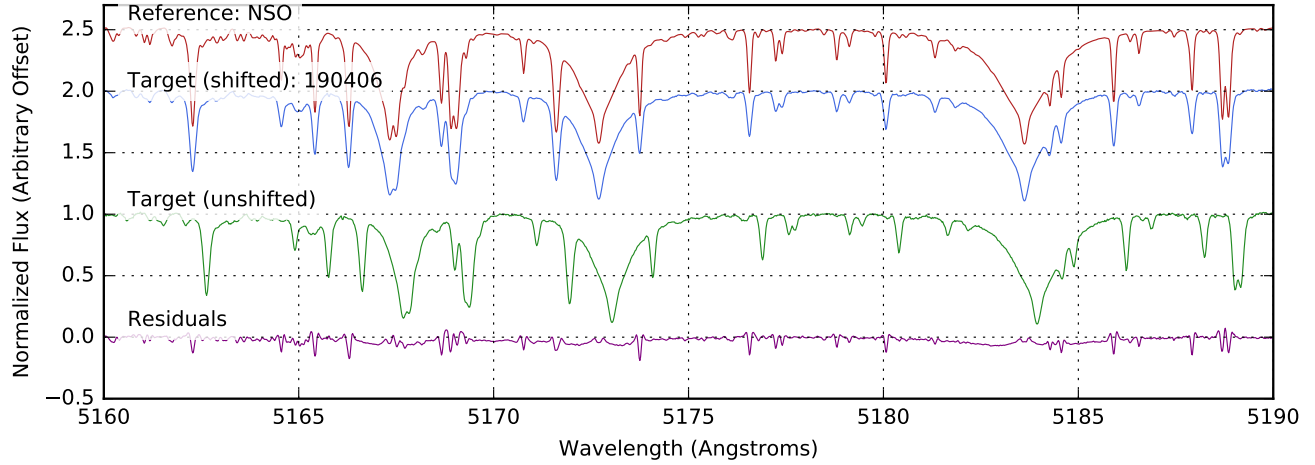


Figure 3. Solar reference spectrum and spectrum of HD190406 (spectral type G0V) before and after registration (see § 3.1).

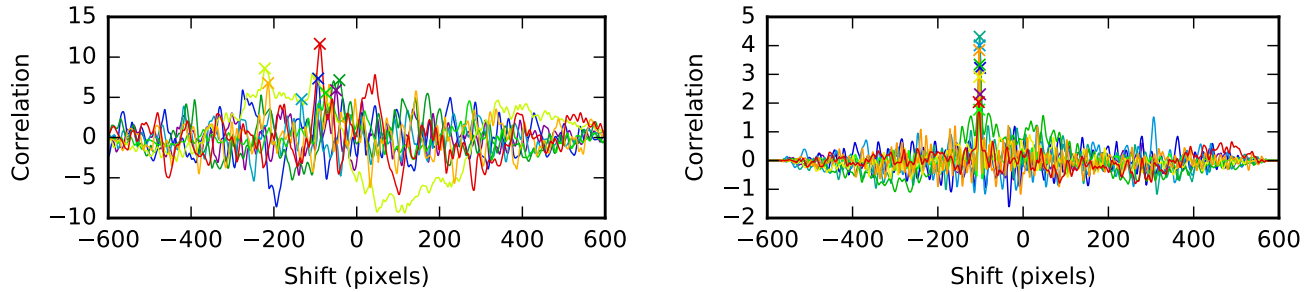


Figure 4. Cross-correlation of the different segments in a single order of the spectrum of Barnard's star (GL669, spectral type M4V), against the solar spectrum (left) and an M dwarf spectrum (right). Due to the dissimilarity in spectra, the cross-correlation with the solar spectrum gives multiple peaks which do not correspond to the true shift, whereas the previously-shifted M dwarf spectrum serves as a better reference (see § 3.1).

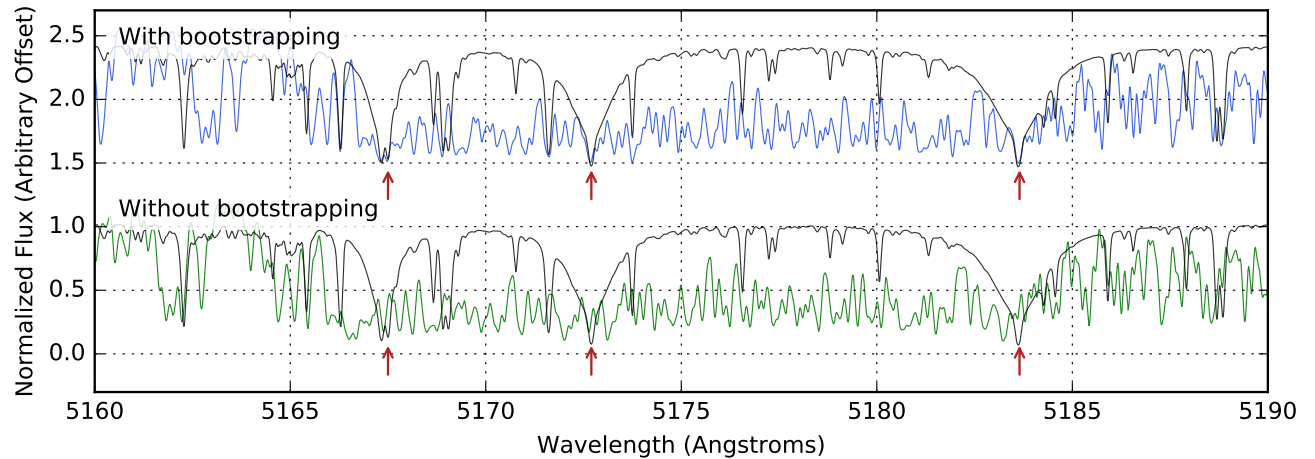


Figure 5. Spectrum of Barnard's star (GL669, spectral type M4V) when shifted against the solar spectrum (bottom) and against a previously shifted template M dwarf spectrum (top). The solar spectrum, which was chosen to be the library rest wavelength scale, is overlaid in gray. Red arrows indicate specific spectral features which are properly aligned only when the target spectrum is shifted against the M dwarf reference. Using the bootstrapping approach described in § 3.1 to derive a ladder of wavelength standards of different spectral types, we achieve superior spectral registration.

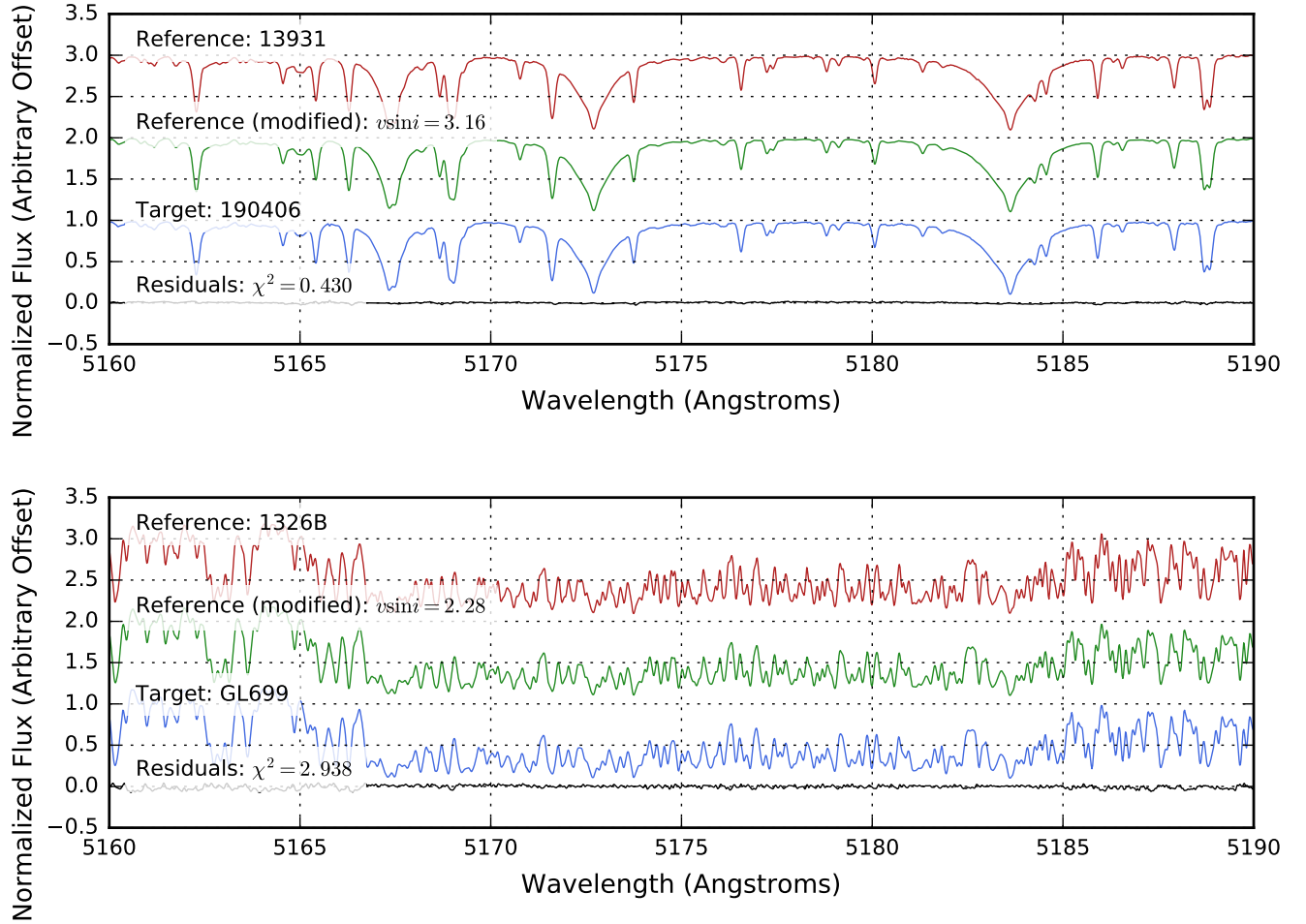


Figure 6. Best matching library spectra to HD190406 (top) and GL699 (bottom). The modified reference spectra are the library spectra after applying a broadening kernel and fitting a cubic spline to the continuum (see § 3.2).

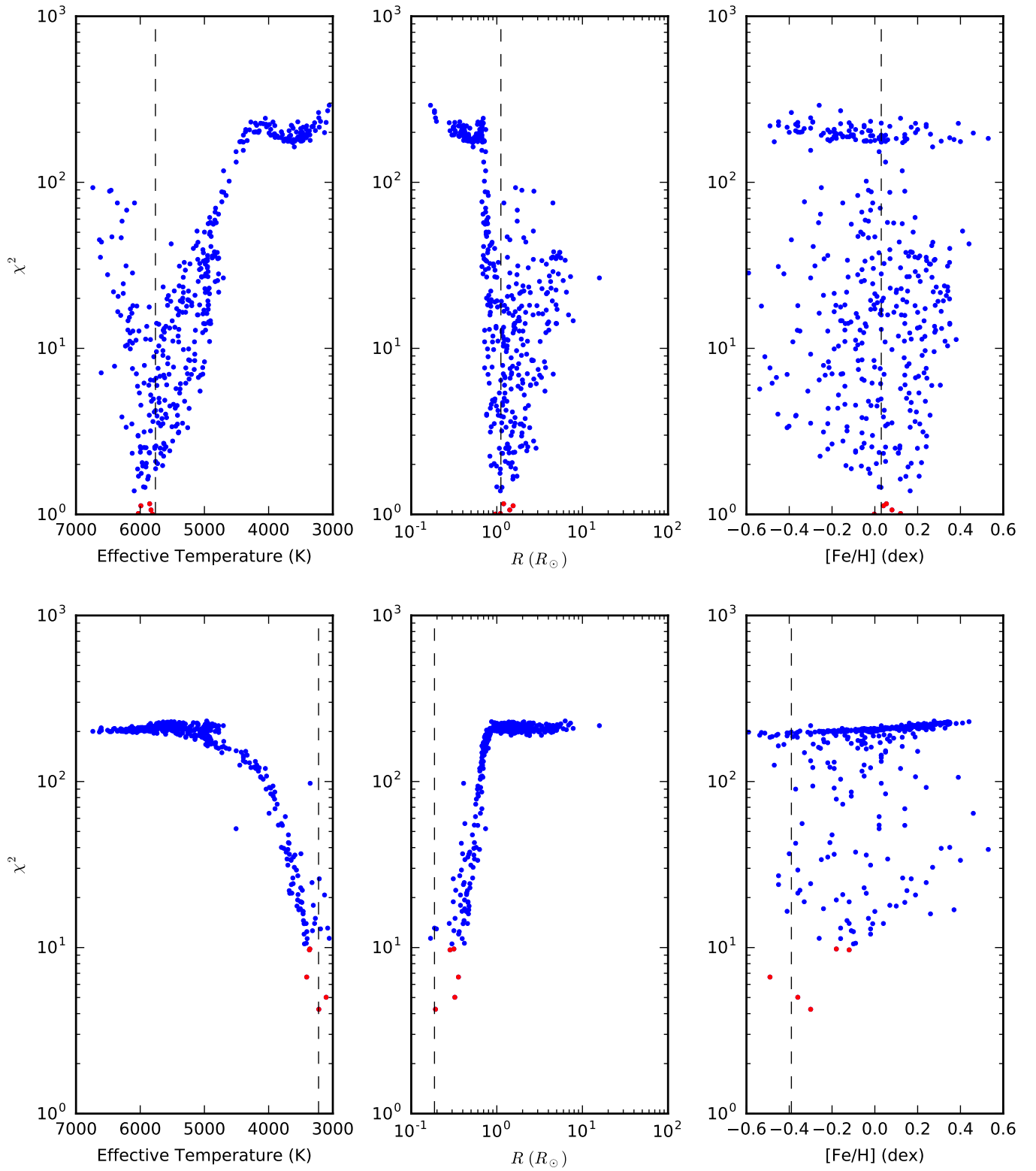


Figure 7. Best chi-squared values for the matches between the spectrum of HD190406 (top) and GL699 (bottom) with each library spectrum, plotted against the library star parameters (see § 3.2). The stars with the five lowest chi-squared values are displayed in red, and we see that there is a sharp minimum in chi-squared close to the true target parameters, indicated with a vertical line. This match was performed in the wavelength region 5300 - 5400 Å.

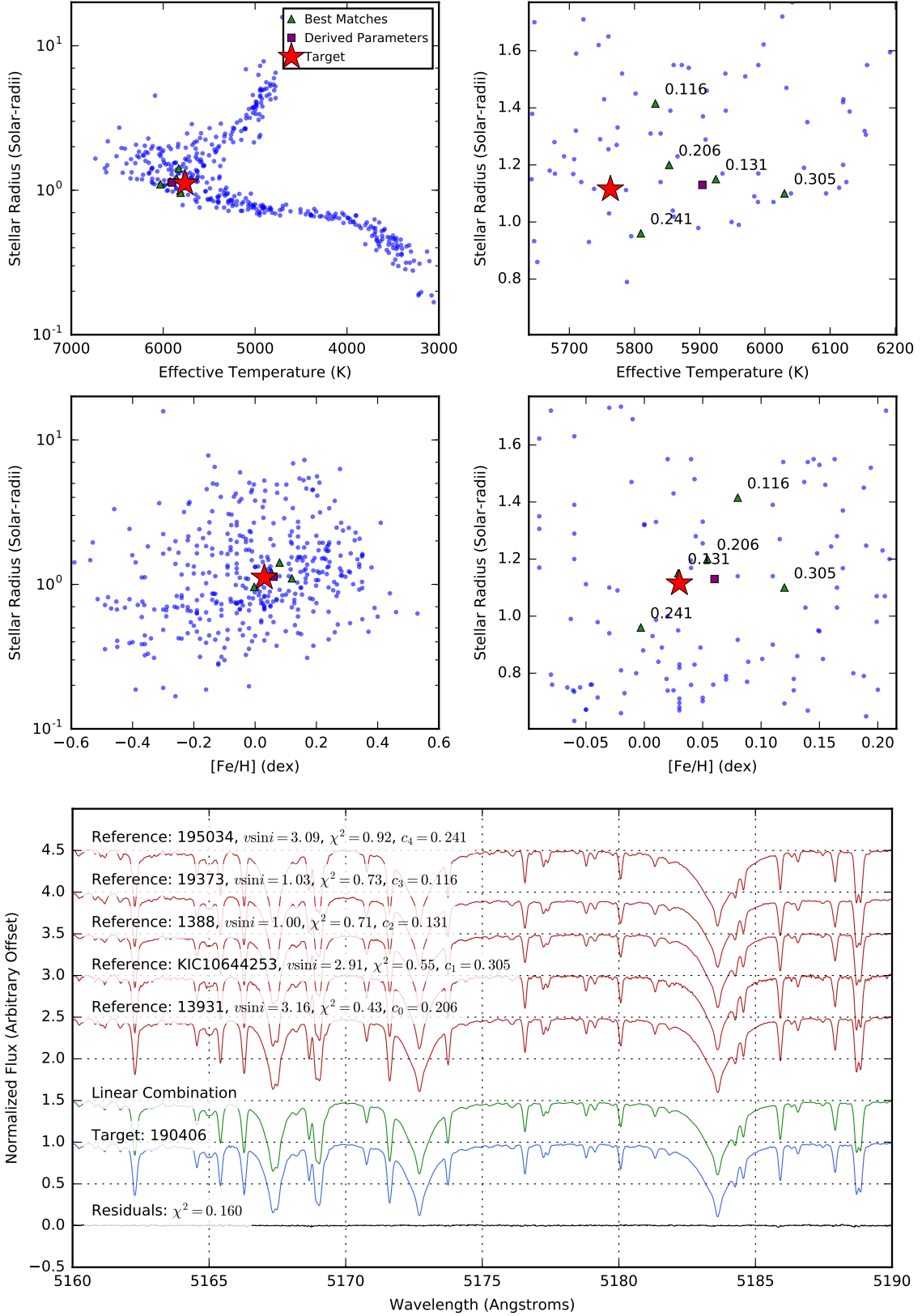


Figure 8. Results from the linear combination approach (§ 3.3) for the star HD190406. Top: The position of the five reference stars used, with their respective coefficients. The star indicates the library parameters of the target, while the purple square denotes the weighted average of the reference parameters. Bottom: The reference spectra and linear combination found. The final χ^2 of 0.160 for the linear combination is lower than the χ^2 for the best matching single spectrum, $\chi^2 = 0.43$.

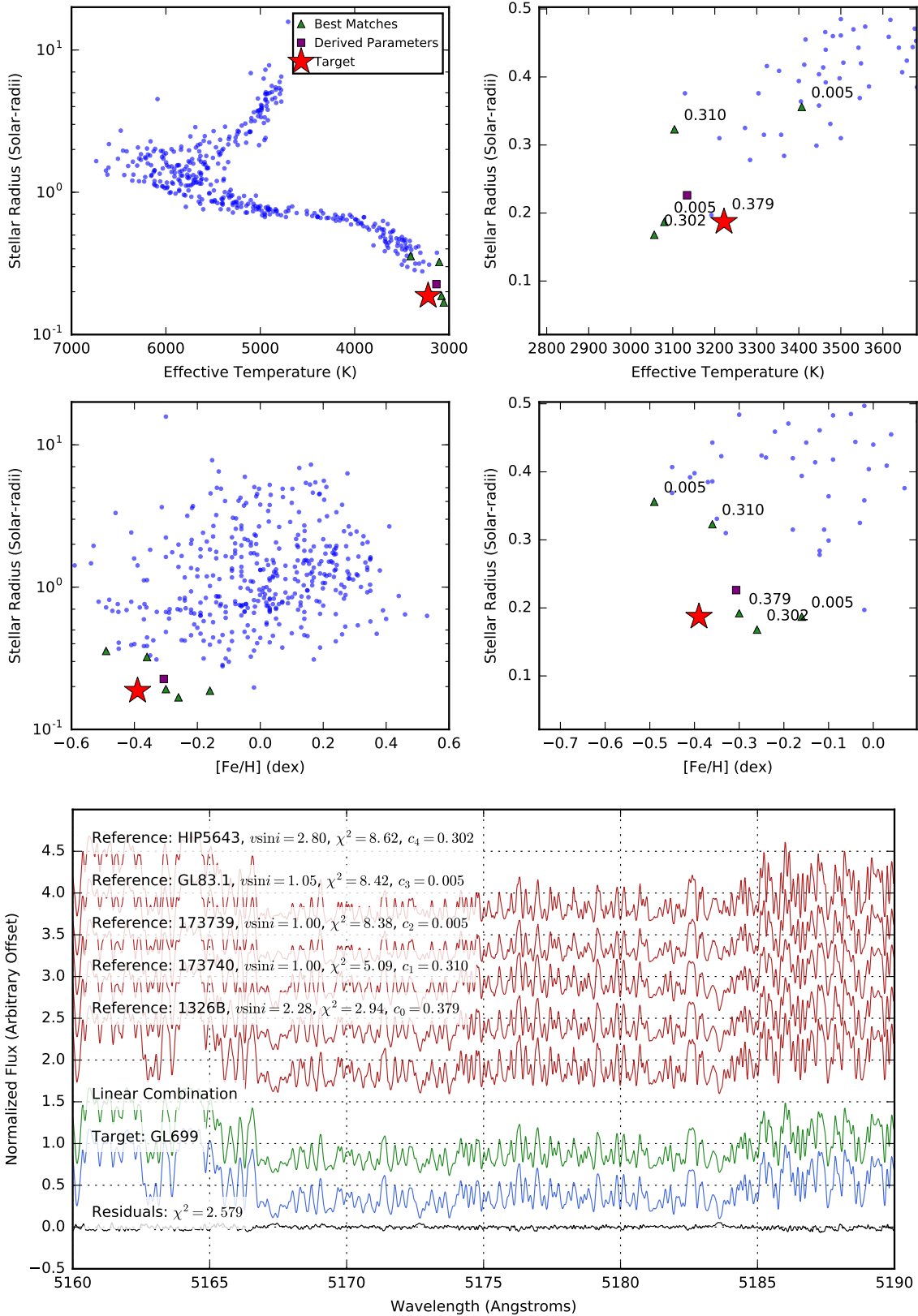


Figure 9. Same as Figure 8, but for the star GL699. The final residuals between the target star and linear combination vanish almost completely (see § 3.3).

To assess the accuracy of the `SpecMatch-Emp`, we performed an internal cross-validation, where we treated each star in the library as an unknown target and ran `SpecMatch-Emp` to compute their parameters from the remaining library spectra. We then compared these derived parameters to their library values. The difference between the derived parameters and the library parameters reflects the errors in the `SpecMatch-Emp` algorithm and in the library parameters.

Figure 10 shows the results of this validation process. We notice a general tendency for the residuals to be most negative for larger values of the derived parameter, and most positive for smaller values. This can be partly explained by the fact that our library spectra are not on an infinite grid, but occupy only a finite region of parameter space. Target stars must necessarily match stars on the interior of that space, resulting in their derived parameters pulled toward the interior of the distribution. On the one hand, this effect amounts to a source of systematic uncertainty resulting from the use of real spectra of nearby stars, as opposed to using model spectra which can be synthesized with arbitrary properties. On the other hand, `SpecMatch-Emp` guards against returning combinations of parameters that are not realized among nearby stars, whereas spectral synthesis may wander into unphysical parameter space.

We attempt to mitigate the regression toward the mean effect by recalibrating the derived parameters. The effect is most pronounced for the residuals in $[\text{Fe}/\text{H}]$, and we fit a first order polynomial to the residuals, obtaining the following correction:

$$[\text{Fe}/\text{H}]_{cal} = 1.240[\text{Fe}/\text{H}]_{SM} - 0.0018 \quad (1)$$

We perform a similar detrending for R_* , but restrict the fit only to derived parameters of $1.0 < R_*/R_\odot < 2.0$, where the effect is most pronounced. For other values of R_* , the library stars are restricted to a narrow region of the HR diagram, so the derived parameters are also confined to a narrow range. However, the main sequence is relatively broad for main sequence stars with $T_{\text{eff}} > 5500$ K and $R_* = 1-2 R_\odot$, so we see a larger spread of derived R_* values and the regression to the mean effect is more pronounced.

The empirical relation we used to recalibrate the derived radii is given in Equation 2. In this case, the calibration relation is quadratic, as we are fitting out a trend in $\Delta R/R$.

$$R_{*,cal} = 0.560R_{*,SM}^2 + 0.165R_{*,SM} \quad (2)$$

The final, detrended results are shown in Figure 11. For all our library stars, the differences between the derived and library values had a scatter of 100 K in T_{eff} , 15% in R_* , and 0.09 dex in $[\text{Fe}/\text{H}]$. These values, listed in Table 3, are the uncertainties which should be

adopted for the output of `SpecMatch-Emp`.

When restricting our analysis to the cool stars (Figure 12), with $T_{\text{eff}} < 4500$ K, the performance of `SpecMatch-Emp` improves to 70 K in T_{eff} , 10% in R_* , and 0.12 dex in $[\text{Fe}/\text{H}]$. For cool stars, most of the stars are from the Mann et al. (2015) sample, which has a median uncertainty of 70 K in T_{eff} , 15% in R_* and 0.09 dex in $[\text{Fe}/\text{H}]$. In this region then, the accuracy of `SpecMatch-Emp` of the routine appears to be primarily limited by the uncertainties in the library parameters, which set the theoretical accuracy limit.

	$\sigma(T_{\text{eff}})$	$\sigma(\Delta R_*/R_*)$	$\sigma([\text{Fe}/\text{H}])$
	K	%	dex
All stars	100	15	0.09
$T_{\text{eff}} < 4500$ K	70	10	0.12
$T_{\text{eff}} \geq 4500$ K	110	16	0.08

Table 3. RMS difference between `SpecMatch-Emp`-derived and library parameters for each star. Different uncertainties may be adopted for stars from different regions of the HR diagram, as the accuracy of `SpecMatch-Emp` depends on the distribution of library stars in that region as well as the scatter of the library parameters for those stars.

4.2. Performance at Low SNR

We also investigated the effect of photon shot noise on the precision of the `SpecMatch-Emp` derived parameters. We chose a subset of 22 stars from the library, distributed across the HR diagram and with original SNR $> 160/\text{pixel}$. Their unshifted spectra are then degraded to lower SNR by injecting Gaussian noise into the raw spectra. We chose target SNRs of 120, 80, 40, 20, and 10 per HIRES pixel. For each target spectrum and SNR level we generated 20 noisy spectra. We then analyzed these spectra through the `SpecMatch-Emp` routine and compared the final properties to those derived from the original high-SNR spectra.

Figure 13 shows the RMS difference between the noisy derived parameters and the high-SNR derived parameter, for each star and target SNR. Treating the high-SNR parameter as the ground truth, these results are representative of the random errors of the derived parameters caused by noise in the input spectrum. As expected, the median scatter increases as the SNR decreases. Nonetheless, the median scatter is only 10.4 K in T_{eff} , 1.7 % in R_* , and 0.008 dex in $[\text{Fe}/\text{H}]$ even at an SNR = 10/pixel. These are significantly smaller than the algorithmic limitations in accuracy from the matching process, demonstrating the robustness of the `SpecMatch-Emp` algorithm even at low SNRs. Table 4 lists the scatter in each parameter at different SNRs.

Furthermore, we note that the increase in scatter with noise is greater for stars with higher T_{eff} and radius.

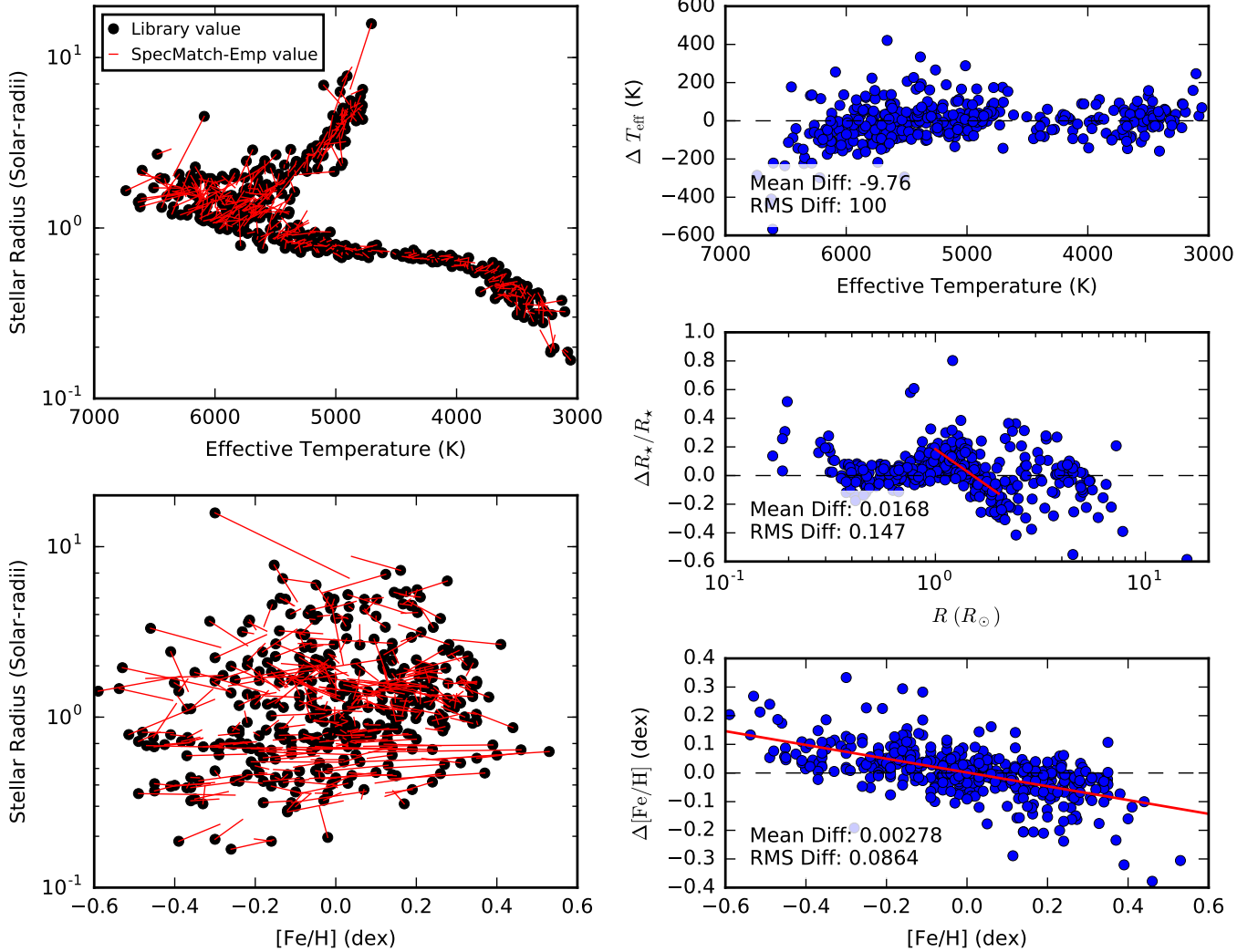


Figure 10. Comparison of library parameters to SpecMatch-derived parameters for each library spectrum in the validation process (§ 4.1). Left: Black points indicate the library stellar parameters, while red lines point to the SpecMatch parameters. Right: Differences between the library values of T_{eff} , R_* , $[\text{Fe}/\text{H}]$ and the derived values. The red lines show the trends in the residuals which we attempt to fit out.

These stars have fewer spectral lines, so random noise has a bigger impact on the derived parameters. The cooler, small stars have much more spectral information in the wavelength region, and so SpecMatch-Emp is more robust to noise for these spectra.

4.3. Performance at Low Spectral Resolution

The library spectra were observed with uniform spectral resolution of $R \approx 60000$. Here, we investigate the effect of lower spectral resolutions on the accuracy of the derived parameters. As spectral resolution decreases and narrow lines become washed out, we expect the performance of SpecMatch-Emp to worsen since the algorithm relies on matching large numbers of spectral lines against the library spectra.

To perform this study, we use the same subset of

	$\sigma(T_{\text{eff}})$	$\sigma(\Delta R_*/R_*)$	$\sigma([\text{Fe}/\text{H}])$
SNR	K		dex
120	3.4	0.004	0.002
80	3.5	0.006	0.003
40	4.9	0.008	0.004
20	6.5	0.012	0.004
10	10.4	0.017	0.008

Table 4. RMS scatter in derived parameters at different signal-to-noise ratios.

22 stars as in Section 4.2 and simulate lower spectral resolution by convolution with a Gaussian kernel. The degraded spectra were then passed through the SpecMatch-Emp routine and a final set of properties was obtained.

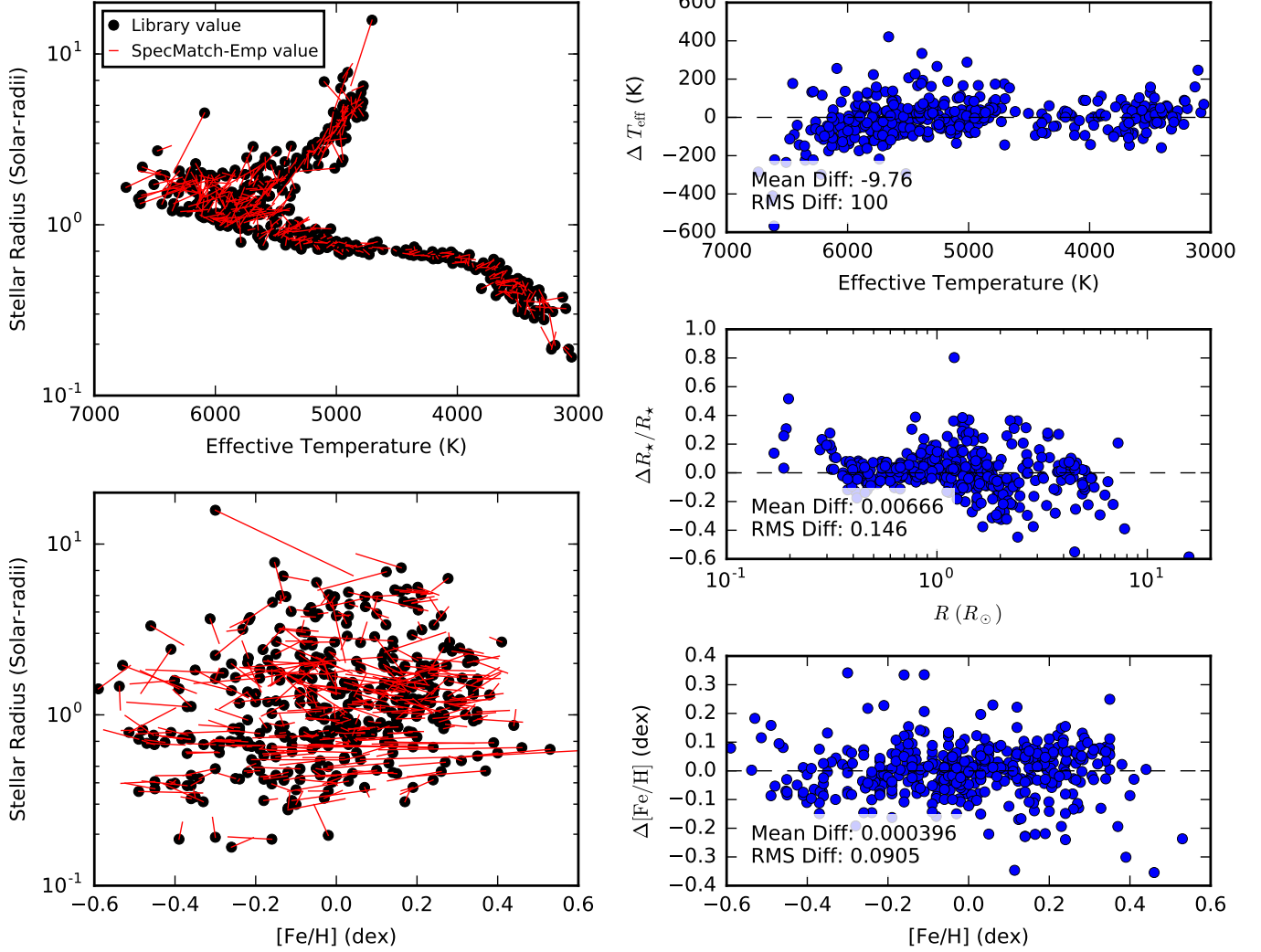


Figure 11. Same as 10, but after performing detrending (see § 4.1).

Just as in the previous section, we treat the properties obtained using the original high-resolution ($R \approx 60000$) spectra as the ground truth. We plot the absolute difference between these properties and the derived properties from each degraded spectrum in Figure 14. The scatter remains small down to $R = 30000$, with a median of 10 K in T_{eff} , 1.3% in R_* , and 0.014 dex in $[\text{Fe}/\text{H}]$. At $R = 20000$, the scatter due to the decreased resolution becomes comparable in size to the algorithmic uncertainties determined through our cross validation study (Section 4.1). At even lower resolutions, SpecMatch-Emp is no longer usable, producing very large errors particularly in T_{eff} and R_* . Table 5 summarizes these results.

A closer analysis of the intermediate results reveals that the spectral registration step is fairly insensitive to lower spectral resolution. The same shift results, accurate to approximately one pixel, are obtained for most orders even at $R = 10000$.

	$\sigma(T_{\text{eff}})$	$\sigma(\Delta R_*/R_*)$	$\sigma([\text{Fe}/\text{H}])$
R	K		dex
50000	10.1	0.015	0.009
30000	10.4	0.013	0.014
20000	71.1	0.041	0.045
10000	424	0.13	0.092
5000	962	2.28	0.094

Table 5. Median scatter in derived parameters at different spectral resolutions.

The performance of SpecMatch-Emp suffers during the matching step. In the current implementation of SpecMatch-Emp, we do not account for the spectrometer instrumental profile. As a result, at lower resolution, the algorithm favors increased rotational broadening to account for the broader lines. This compensation by higher rotational broadening works well down

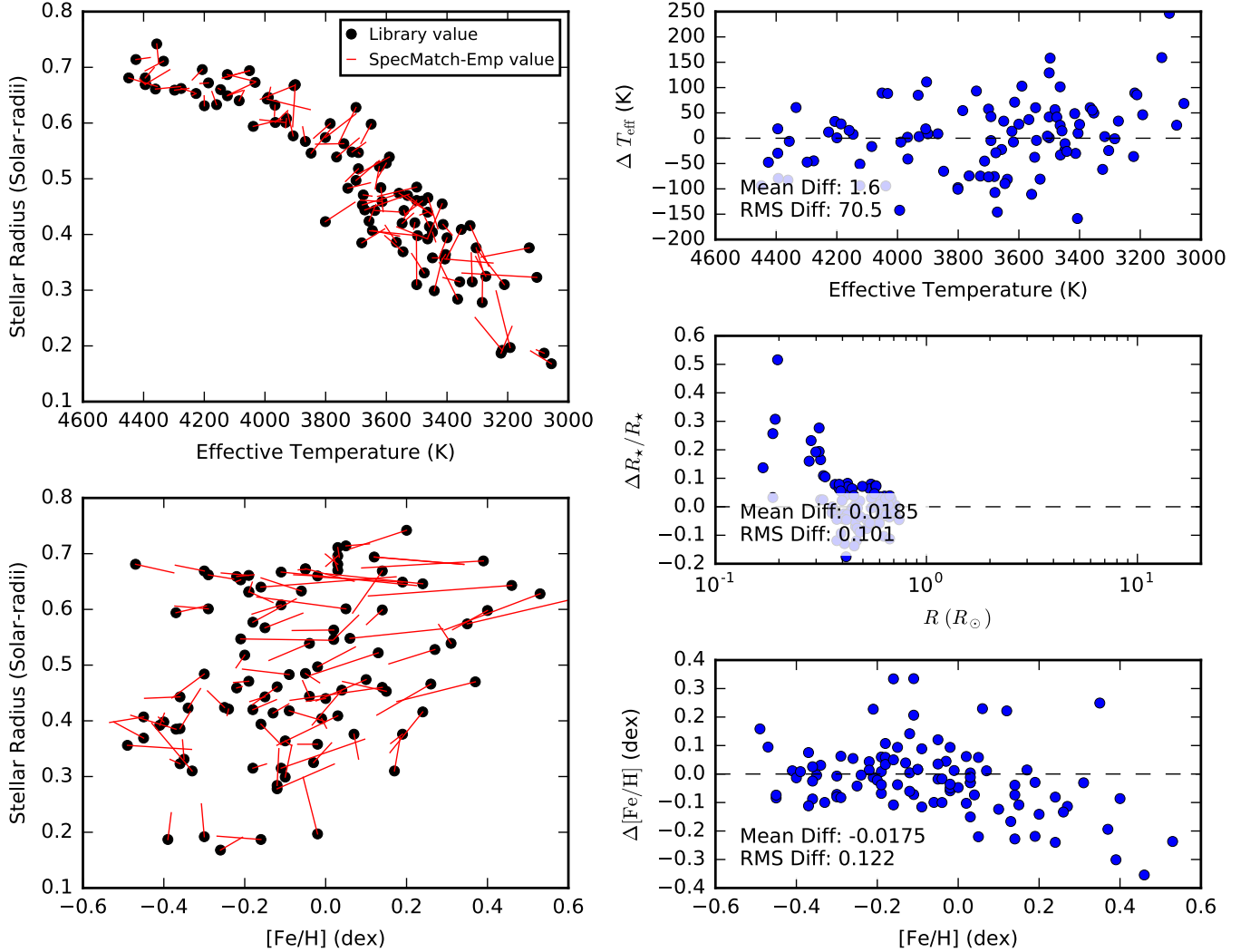


Figure 12. Same as 11, but for the library stars with $T_{\text{eff}} < 4500$ K. Performance is improved for this selection of stars due to the more limited spread in main sequence stellar parameters in the HR diagram (see § 4.1).

to $R \approx 20000$, beyond which it fails for two reasons. First, the kernels associated with rotational broadening and the instrumental profile are different. Second, during the matching step, we do not allow the broadening kernel to exceed a $v \sin i > 10 \text{ km s}^{-1}$. At a resolution of ~ 10000 the instrumental profile has a width of $\sim 13 \text{ km s}^{-1}$, which is above the maximum $v \sin i$ allowed during our fitting.

As a result, at spectral resolutions below 20000, no reference spectrum can be broadened sufficiently to simulate the wider point-spread function of the spectrometer, and the matching algorithm produces a large number of similarly poor matches. The χ^2 surfaces no longer have sharp minima and the final parameters obtained are less accurate. This decrease in performance particularly affects stars with low T_{eff} and R_* . These M and K dwarfs have many narrow but overlapping lines in their spectra (e.g. Figure 3), which get smeared out into a continuum

as the resolution decreases, preventing accurate matching with the library spectra. The spectra from hotter stars have fewer but broader lines which remain visible even in lower resolution spectra.

While we have made no explicit treatment of of spectrometer instrumental broadening, the current implementation of `SpecMatch-Emp` is relatively insensitive to spectral resolutions down to $R \approx 30000$. Difficulties in modeling spectra with $R \lesssim 20000$ could be addressed by proper treatment of the instrumental broadening profile. We welcome community contributions in this respect.

5. CONCLUSIONS

We have compiled a library of high resolution, high signal-to-noise optical spectra of 404 touchstone stars with well-measured properties. The `SpecMatch-Emp` routine is able to rapidly extract fundamental properties of a star from its optical spectrum by compari-

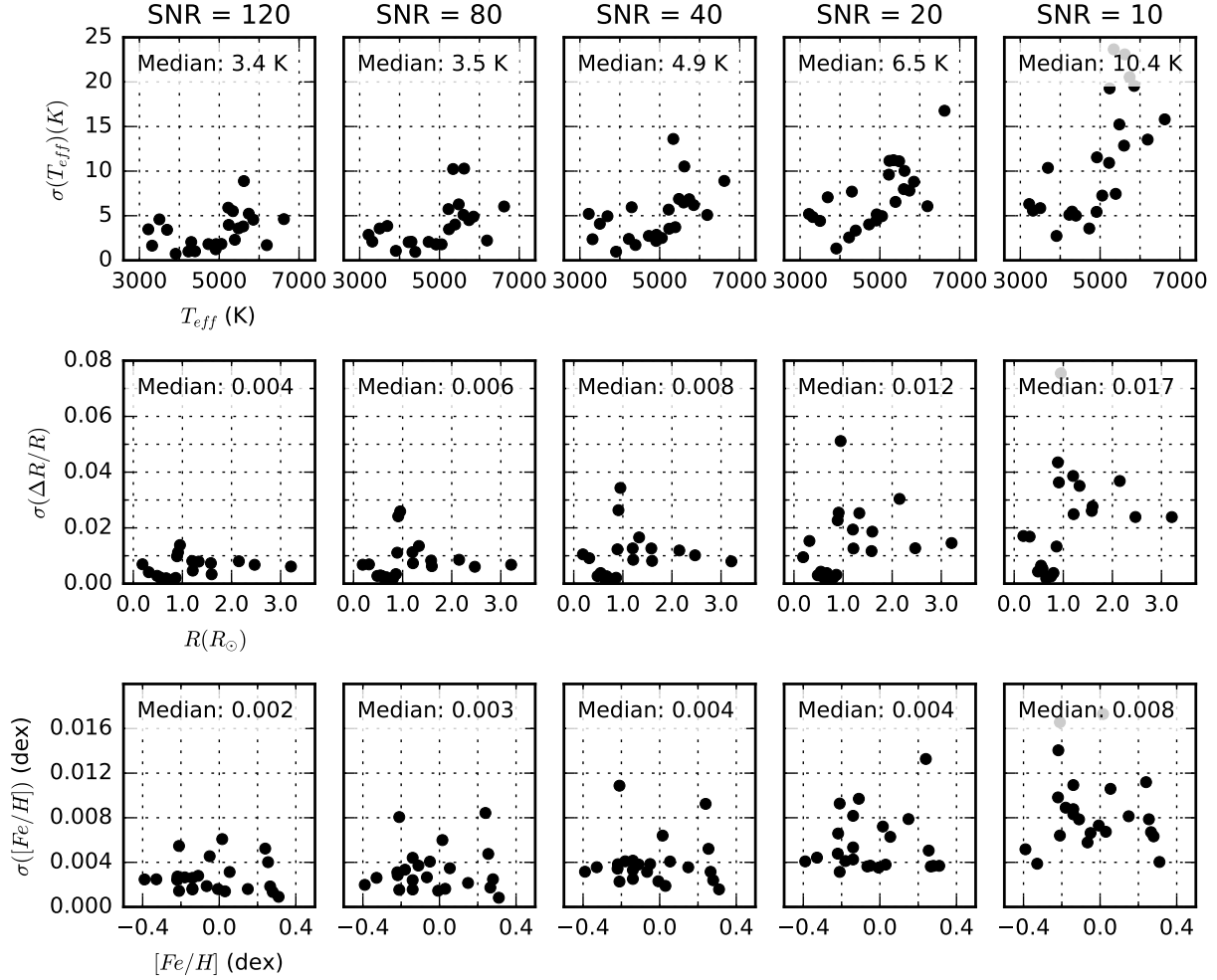


Figure 13. Scatter of SpecMatch-derived parameters as a function of SNR of the target spectrum, from the noise study described in § 4.2. Each point represents the median RMS difference between the parameters derived from 20 noisy spectra, and the derived parameter of the original, high SNR spectrum. As SNR decreases, the median scatter increases, and is representative of the effect of photon noise on the precision of SpecMatch-Emp. The decrease in precision is most pronounced for stars with greater T_{eff} and radius, as these stars have fewer spectral lines and are thus most susceptible to features being washed out by noise.

son against this library. The density of the library and the quality of the associated stellar parameters enables SpecMatch-Emp to achieve accuracies of 100 K in T_{eff} , 15% in R_{\star} and 0.09 dex in $[Fe/H]$. By incorporating information from across a large wavelength range, the algorithm is relatively robust to photon noise and can readily be applied to stellar spectra with signal-to-noise ratios as low as 10 per pixel. The algorithm also remains robust at lower spectral resolutions until about $R \sim 20000$.

A key advantage of SpecMatch-Emp is its accuracy for cool stars with $T_{\text{eff}} < 4500$ K. By using empirical, rather than synthetic, spectra to create the library, we have bypassed the difficulties that existing spectral synthesis codes have in modeling the complex spectra of

cool stars. Instead, the rich spectral information contained in these stars’ spectra is an advantage during the matching process, as the greater number of features improves both the accuracy and precision of the derived parameters. We expect that SpecMatch-Emp will be a valuable tool for efficiently characterizing large numbers of late-type stars. Such characterization work will be a key observational follow-up effort for future transit surveys such as *TESS* (Ricker et al. 2014) that have an emphasis on M-stars.

The applicability of SpecMatch-Emp is only valid within the region of stellar parameter space spanned by our library stars, i.e. SpecMatch-Emp is not applicable to rapidly-rotating stars, young stars, chemically peculiar stars, extremely metal-poor stars, etc. Furthermore, the

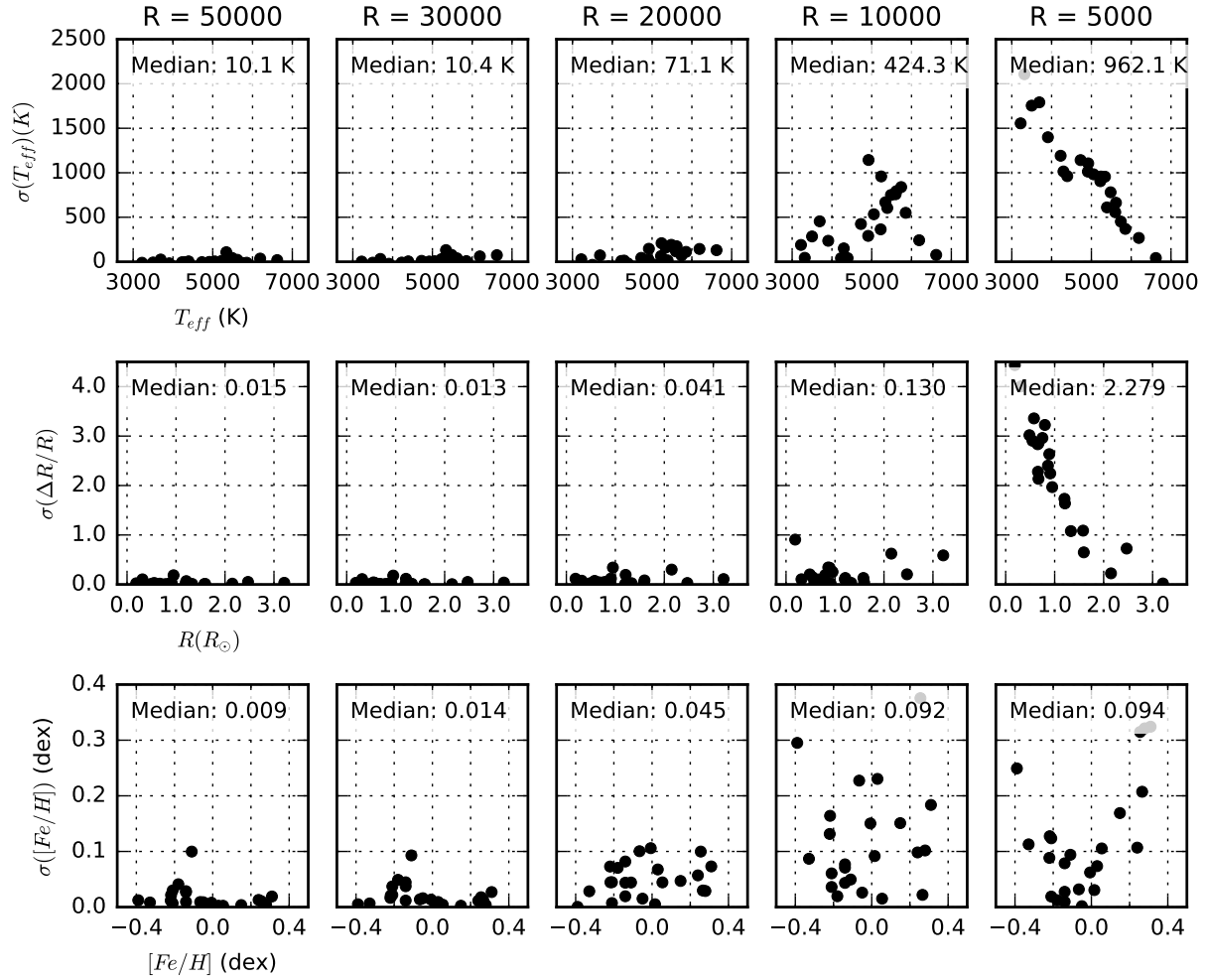


Figure 14. Absolute difference between the parameters derived from the spectra with degraded spectral resolution and those derived from the original high-resolution spectra, analogous to figure 13. *SpecMatch-Emp* remains accurate down to $R \approx 30000$, beyond which the performance degrades rapidly (see § 4.3).

routine’s accuracy is limited by the quality of the input parameters. Because the library stars are drawn from the sample of nearby stars, we anticipate that their parameters will be refined with future observations. The *SpecMatch-Emp* library may be easily updated to include these updated parameters, with no modifications to the algorithm.

We thank Tabetha Boyajian, John Brewer, Debra Fischer, Eric Gaidos, Andrew Howard, Howard Isaacson, Heather Knutson, Andrew Mann, and Geoffrey Marcy for enlightening conversations that improved this manuscript. We thank the many observers who collected the Keck/HIRES data used here including R. Paul Butler, Debra A. Fischer, Benjamin J. Fulton, Andrew W. Howard, Howard Isaacson, John A. Johnson, Geoffrey W. Marcy, Kathryn M. G. Peek, Benjamin J. Ful-

ton, Steven S. Vogt, Lauren M. Weiss, and Jason T. Wright. S. W. Y. acknowledges support through the Caltech Summer Undergraduate Research Fellowship program. E. A. P. acknowledges support from a Hubble Fellowship grant HST-HF2-51365.001-A awarded by the Space Telescope Science Institute, which is operated by the Association of Universities for Research in Astronomy, Inc. for NASA under contract NAS 5-26555. This work has made use of data from the European Space Agency (ESA) mission *Gaia* (<http://www.cosmos.esa.int/gaia>), processed by the *Gaia* Data Processing and Analysis Consortium (DPAC, <http://www.cosmos.esa.int/web/gaia/dpac/consortium>). Funding for the DPAC has been provided by national institutions, in particular the institutions participating in the *Gaia* Multilateral Agreement. Some of the data presented herein were obtained at the W. M. Keck Observatory,

which is operated as a scientific partnership among the California Institute of Technology, the University of California and the National Aeronautics and Space Administration. The Observatory was made possible by the generous financial support of the W. M. Keck Foundation. Finally, the authors wish to recognize and acknowledge the very significant cultural role and reverence that the summit of Maunakea has always had within the indigenous Hawaiian community. We are most fortunate to have the opportunity to conduct observations from this mountain.

APPENDIX
A. LIBRARY STARS

Table A1. SpecMatch Library

Name	T_{eff} K	R_{\star} R_{\odot}	$\log g$ dex	[Fe/H] dex	M_{\star} M_{\odot}	$\log_{10}(\text{age})$	π_{\star} mas	V mag	Notes
HD 100623	5140 ± 60	0.720 ± 0.040	4.56 ± 0.05	-0.36 ± 0.05	0.75 ± 0.04	9.81 ± 0.50	104.6	6.0	A1
HD 101904	5883 ± 60	1.540 ± 0.190	4.10 ± 0.05	0.12 ± 0.05	1.12 ± 0.09	9.80 ± 0.11	12.5	8.2	A1
HD 102195	5277 ± 60	0.850 ± 0.050	4.50 ± 0.05	0.10 ± 0.05	0.89 ± 0.04	9.74 ± 0.49	34.0	8.1	A1
HD 102444	5227 ± 60	2.670 ± 0.390	3.60 ± 0.05	-0.00 ± 0.05	1.02 ± 0.21	9.98 ± 0.27	8.5	8.0	A1
HD 102956	4985 ± 60	3.790 ± 0.470	3.38 ± 0.05	0.26 ± 0.05	1.30 ± 0.15	9.70 ± 0.17	8.1	7.9	A1
HD 103459	5722 ± 60	1.710 ± 0.210	4.03 ± 0.05	0.24 ± 0.05	1.15 ± 0.12	9.81 ± 0.15	16.0	7.6	A2
HD 103890	6120 ± 60	1.430 ± 0.160	4.19 ± 0.05	0.03 ± 0.05	1.17 ± 0.07	9.63 ± 0.09	13.7	8.0	A1
HD 104437	5761 ± 60	1.030 ± 0.090	4.40 ± 0.05	0.17 ± 0.05	1.03 ± 0.04	9.64 ± 0.35	16.6	8.6	A1
HD 106088	5470 ± 60	2.070 ± 0.260	3.87 ± 0.05	0.34 ± 0.05	1.23 ± 0.12	9.75 ± 0.13	10.3	8.4	A1
HD 107181	5628 ± 60	1.640 ± 0.210	4.05 ± 0.05	0.31 ± 0.05	1.13 ± 0.12	9.86 ± 0.15	12.5	8.4	A1
HD 108189	5373 ± 60	2.890 ± 0.410	3.56 ± 0.05	0.03 ± 0.05	1.15 ± 0.21	9.81 ± 0.23	7.5	7.7	A1
HD 108863	4878 ± 60	5.590 ± 0.660	3.08 ± 0.05	0.20 ± 0.05	1.37 ± 0.14	9.61 ± 0.15	5.8	7.7	A1
HD 109159	5151 ± 60	2.570 ± 0.320	3.60 ± 0.05	-0.08 ± 0.05	0.93 ± 0.13	10.09 ± 0.17	9.7	8.0	A1
HD 109749	5825 ± 60	1.310 ± 0.150	4.24 ± 0.05	0.24 ± 0.05	1.10 ± 0.08	9.78 ± 0.13	15.9	8.1	A1
HD 10995	5688 ± 60	2.870 ± 0.340	3.67 ± 0.05	0.10 ± 0.05	1.45 ± 0.19	9.50 ± 0.17	11.0	7.3	A1
HD 110463	4906 ± 60	0.760 ± 0.030	4.55 ± 0.05	0.06 ± 0.05	0.80 ± 0.04	9.73 ± 0.52	44.1	8.3	A1
HD 110537	5718 ± 60	1.140 ± 0.110	4.30 ± 0.05	0.08 ± 0.05	0.99 ± 0.04	9.92 ± 0.13	21.5	7.8	A2
HD 110743	5198 ± 60	0.840 ± 0.050	4.47 ± 0.05	0.01 ± 0.05	0.84 ± 0.04	9.98 ± 0.40	22.9	8.8	A2
HD 110833	4999 ± 60	0.800 ± 0.040	4.51 ± 0.05	0.18 ± 0.05	0.83 ± 0.04	9.86 ± 0.50	66.4	7.0	A2
HD 111814	5646 ± 60	1.940 ± 0.240	3.93 ± 0.05	0.22 ± 0.05	1.20 ± 0.11	9.76 ± 0.14	12.4	8.1	A1
HD 112415	5574 ± 60	1.230 ± 0.130	4.25 ± 0.05	0.28 ± 0.05	1.00 ± 0.06	9.99 ± 0.13	14.8	8.7	A1
HD 112914	4816 ± 60	0.700 ± 0.030	4.51 ± 0.05	-0.26 ± 0.05	0.71 ± 0.03	10.00 ± 0.45	41.4	8.6	A2
HD 114659	4838 ± 60	5.450 ± 0.720	3.08 ± 0.05	0.17 ± 0.05	1.34 ± 0.20	9.64 ± 0.22	5.1	8.3	A1
HD 116442	5155 ± 60	0.720 ± 0.040	4.54 ± 0.05	-0.38 ± 0.05	0.74 ± 0.04	9.88 ± 0.49	59.7	7.1	A1
HD 122253	5007 ± 60	3.780 ± 0.520	3.36 ± 0.05	0.03 ± 0.05	1.24 ± 0.21	9.72 ± 0.25	9.0	7.8	A1
HD 122973	5989 ± 60	1.070 ± 0.060	4.46 ± 0.05	0.20 ± 0.05	1.12 ± 0.04	9.20 ± 0.25	20.6	8.1	A2
HD 123239	4795 ± 60	5.960 ± 0.890	2.94 ± 0.05	-0.05 ± 0.05	1.18 ± 0.24	9.78 ± 0.29	6.5	8.4	A2
HD 124257A	5911 ± 60	1.460 ± 0.160	4.15 ± 0.05	0.15 ± 0.05	1.13 ± 0.08	9.76 ± 0.11	8.7	9.2	A1
HD 125607	4985 ± 60	3.910 ± 0.510	3.35 ± 0.05	0.10 ± 0.05	1.26 ± 0.18	9.71 ± 0.22	4.8	8.1	A1
HD 126583	5482 ± 60	0.880 ± 0.060	4.49 ± 0.05	-0.00 ± 0.05	0.92 ± 0.04	9.65 ± 0.45	28.7	8.1	A1
HD 128311	4918 ± 60	0.790 ± 0.040	4.49 ± 0.05	0.19 ± 0.05	0.81 ± 0.04	9.95 ± 0.49	60.4	7.4	A2
HD 130048	4964 ± 60	6.290 ± 0.710	3.02 ± 0.05	0.28 ± 0.05	1.52 ± 0.13	9.47 ± 0.13	5.4	7.1	A1
HD 130307	4985 ± 60	0.740 ± 0.040	4.56 ± 0.05	-0.13 ± 0.05	0.78 ± 0.04	9.74 ± 0.51	50.8	7.8	A2
HD 131511	5259 ± 60	0.860 ± 0.060	4.47 ± 0.05	0.13 ± 0.05	0.88 ± 0.04	9.90 ± 0.46	86.7	6.0	A2
HD 131582	4728 ± 60	0.670 ± 0.030	4.52 ± 0.05	-0.33 ± 0.05	0.68 ± 0.03	10.00 ± 0.46	40.9	8.6	A1
HD 132254	6157 ± 60	1.550 ± 0.190	4.14 ± 0.05	0.16 ± 0.05	1.26 ± 0.08	9.56 ± 0.08	39.7	5.6	A1
HD 133125	5506 ± 60	0.860 ± 0.060	4.49 ± 0.05	-0.13 ± 0.05	0.89 ± 0.04	9.71 ± 0.44	17.7	8.8	A2
HD 135101A	5677 ± 60	1.280 ± 0.140	4.20 ± 0.05	0.04 ± 0.05	0.98 ± 0.05	10.01 ± 0.09	30.7	6.7	A1
HD 135872	4992 ± 60	3.370 ± 0.460	3.44 ± 0.05	0.12 ± 0.05	1.16 ± 0.20	9.84 ± 0.25	11.7	7.3	A1
HD 137778	5128 ± 60	0.830 ± 0.050	4.52 ± 0.05	0.27 ± 0.05	0.89 ± 0.04	9.66 ± 0.50	48.1	7.5	A2
HD 13871	6416 ± 60	1.940 ± 0.240	4.03 ± 0.05	0.27 ± 0.05	1.49 ± 0.10	9.34 ± 0.08	24.9	5.8	A2
HD 1388	5925 ± 60	1.150 ± 0.120	4.32 ± 0.05	0.03 ± 0.05	1.06 ± 0.05	9.71 ± 0.21	36.7	6.5	A1
HD 13931	5853 ± 60	1.200 ± 0.120	4.28 ± 0.05	0.05 ± 0.05	1.04 ± 0.05	9.82 ± 0.12	21.4	7.6	A1
HD 144872	4781 ± 60	0.690 ± 0.030	4.52 ± 0.05	-0.25 ± 0.05	0.70 ± 0.03	9.97 ± 0.47	43.1	8.6	A1
HD 14655	5755 ± 60	1.970 ± 0.230	3.92 ± 0.05	0.12 ± 0.05	1.23 ± 0.12	9.70 ± 0.13	9.8	8.2	A2

Table A1 continued

Table A1 (*continued*)

Name	T_{eff} K	R_* R_{\odot}	$\log g$ dex	[Fe/H] dex	M_* M_{\odot}	$\log_{10}(\text{age})$	π_* mas	V mag	Notes
HD 14787	4946 ± 60	4.450 ± 0.590	3.23 ± 0.05	0.03 ± 0.05	1.28 ± 0.20	9.67 ± 0.23	8.4	7.6	A1
HD 148284	5572 ± 60	1.800 ± 0.240	3.97 ± 0.05	0.16 ± 0.05	1.11 ± 0.12	9.88 ± 0.16	8.0	9.0	A1
HD 14855	5023 ± 60	3.430 ± 0.480	3.43 ± 0.05	0.03 ± 0.05	1.17 ± 0.21	9.81 ± 0.26	11.8	7.4	A1
HD 149750	5802 ± 60	1.450 ± 0.180	4.14 ± 0.05	0.19 ± 0.05	1.09 ± 0.10	9.85 ± 0.14	11.5	8.6	A1
HD 1502	4947 ± 60	4.910 ± 0.610	3.18 ± 0.05	0.10 ± 0.05	1.33 ± 0.18	9.64 ± 0.19	6.0	8.3	A2
HD 150706	5949 ± 60	1.000 ± 0.050	4.53 ± 0.05	0.02 ± 0.05	1.06 ± 0.04	9.19 ± 0.24	35.4	7.0	A1
HD 152581	5027 ± 60	3.710 ± 0.410	3.29 ± 0.05	-0.21 ± 0.05	0.94 ± 0.06	10.06 ± 0.11	6.0	8.3	A1
HD 152733	4835 ± 60	5.260 ± 0.690	3.10 ± 0.05	0.16 ± 0.05	1.30 ± 0.18	9.69 ± 0.21	6.1	8.1	A1
HD 15336	5025 ± 60	4.560 ± 0.570	3.12 ± 0.05	-0.16 ± 0.05	1.00 ± 0.12	9.97 ± 0.17	2.9	8.9	A1
HD 153525	4826 ± 60	0.740 ± 0.030	4.54 ± 0.05	0.03 ± 0.05	0.78 ± 0.04	9.83 ± 0.51	55.7	7.9	A1
HD 155413	5740 ± 60	2.470 ± 0.280	3.79 ± 0.05	0.27 ± 0.05	1.42 ± 0.11	9.55 ± 0.11	11.6	7.3	A1
HD 155456	5225 ± 60	0.910 ± 0.070	4.43 ± 0.05	0.26 ± 0.05	0.88 ± 0.04	10.02 ± 0.33	28.3	8.3	A1
HD 155712	4911 ± 60	0.750 ± 0.040	4.52 ± 0.05	-0.07 ± 0.05	0.77 ± 0.04	9.91 ± 0.49	48.7	8.0	A2
HD 156846	5999 ± 60	1.880 ± 0.230	4.01 ± 0.05	0.24 ± 0.05	1.35 ± 0.12	9.56 ± 0.11	21.1	6.5	A1
HD 161479	5642 ± 60	1.150 ± 0.120	4.31 ± 0.05	0.28 ± 0.05	1.03 ± 0.06	9.86 ± 0.17	20.4	8.1	A1
HD 162232	5492 ± 60	1.030 ± 0.100	4.36 ± 0.05	0.14 ± 0.05	0.92 ± 0.04	10.04 ± 0.16	13.4	8.6	A2
HD 164922	5341 ± 60	0.950 ± 0.080	4.39 ± 0.05	0.15 ± 0.05	0.88 ± 0.04	10.07 ± 0.18	45.4	7.0	A1
HD 168443	5551 ± 60	1.480 ± 0.180	4.07 ± 0.05	0.04 ± 0.05	0.98 ± 0.06	10.05 ± 0.10	26.4	6.9	A2
HD 170657	5041 ± 60	0.760 ± 0.040	4.54 ± 0.05	-0.12 ± 0.05	0.79 ± 0.04	9.81 ± 0.50	76.2	6.8	A1
HD 17156	5970 ± 60	1.510 ± 0.180	4.15 ± 0.05	0.22 ± 0.05	1.19 ± 0.09	9.67 ± 0.11	30.3	8.2	A1
HD 172051	5636 ± 60	0.830 ± 0.040	4.58 ± 0.05	-0.26 ± 0.05	0.89 ± 0.04	9.34 ± 0.37	77.0	5.9	A2
HD 175425	5773 ± 60	1.270 ± 0.130	4.23 ± 0.05	0.12 ± 0.05	1.03 ± 0.05	9.90 ± 0.11	13.2	7.9	A1
HD 17620	5159 ± 60	3.040 ± 0.400	3.46 ± 0.05	-0.08 ± 0.05	0.96 ± 0.15	10.03 ± 0.20	7.3	8.2	A1
HD 179079	5646 ± 60	1.700 ± 0.220	4.02 ± 0.05	0.23 ± 0.05	1.12 ± 0.11	9.87 ± 0.15	14.1	8.0	A1
HD 181234	5314 ± 60	1.040 ± 0.100	4.35 ± 0.05	0.35 ± 0.05	0.92 ± 0.04	10.08 ± 0.14	20.8	8.6	A1
HD 18143	5101 ± 60	0.880 ± 0.060	4.43 ± 0.05	0.27 ± 0.05	0.86 ± 0.04	10.06 ± 0.29	44.3	7.6	A1
HD 18445	4838 ± 60	0.760 ± 0.030	4.44 ± 0.05	-0.04 ± 0.05	0.76 ± 0.03	10.09 ± 0.30	38.9	7.9	A2
HD 18742	4941 ± 60	5.050 ± 0.810	3.09 ± 0.05	-0.02 ± 0.05	1.20 ± 0.26	9.75 ± 0.30	6.2	7.8	A1
HD 189733	5024 ± 60	0.790 ± 0.040	4.51 ± 0.05	0.07 ± 0.05	0.82 ± 0.04	9.89 ± 0.49	50.4	7.6	A1
HD 190228	5238 ± 60	2.150 ± 0.230	3.72 ± 0.05	-0.22 ± 0.05	0.90 ± 0.05	10.08 ± 0.08	15.8	7.3	A1
HD 190571	4999 ± 60	3.600 ± 0.390	3.31 ± 0.05	-0.22 ± 0.05	0.92 ± 0.05	10.08 ± 0.10	9.8	7.5	A1
HD 193690	5542 ± 60	0.980 ± 0.090	4.41 ± 0.05	0.20 ± 0.05	0.96 ± 0.05	9.83 ± 0.37	14.3	9.4	A1
HD 195034	5810 ± 60	0.960 ± 0.060	4.48 ± 0.05	-0.00 ± 0.05	1.02 ± 0.04	9.39 ± 0.35	35.7	7.1	A1
HD 196124	4833 ± 60	0.740 ± 0.030	4.50 ± 0.05	-0.06 ± 0.05	0.76 ± 0.04	9.98 ± 0.47	33.3	8.9	A1
HD 199255	5027 ± 60	3.740 ± 0.570	3.29 ± 0.05	-0.05 ± 0.05	0.97 ± 0.21	10.02 ± 0.28	8.5	7.3	A2
HD 199381	4844 ± 60	4.610 ± 0.620	3.19 ± 0.05	0.17 ± 0.05	1.21 ± 0.18	9.78 ± 0.21	13.6	6.9	A1
HD 200964	4983 ± 60	4.050 ± 0.590	3.22 ± 0.05	-0.07 ± 0.05	0.96 ± 0.20	10.03 ± 0.27	13.9	6.5	A1
HD 201924	5401 ± 60	0.890 ± 0.070	4.47 ± 0.05	0.05 ± 0.05	0.90 ± 0.04	9.84 ± 0.45	31.9	7.8	A1
HD 202575	4730 ± 60	0.730 ± 0.030	4.50 ± 0.05	-0.02 ± 0.05	0.75 ± 0.03	9.96 ± 0.47	61.8	7.9	A1
HD 203471	5425 ± 60	2.340 ± 0.310	3.72 ± 0.05	-0.02 ± 0.05	1.02 ± 0.18	9.94 ± 0.22	7.7	8.3	A1
HD 203473	5781 ± 60	1.520 ± 0.200	4.11 ± 0.05	0.19 ± 0.05	1.10 ± 0.11	9.86 ± 0.14	13.2	8.2	A1
HD 20367	6094 ± 60	1.100 ± 0.070	4.46 ± 0.05	0.17 ± 0.05	1.14 ± 0.04	9.18 ± 0.22	37.8	6.4	A1
HD 206635	4944 ± 60	2.410 ± 0.240	3.65 ± 0.05	-0.18 ± 0.05	0.87 ± 0.06	10.16 ± 0.04	11.0	8.3	A1
HD 207077	5068 ± 60	3.650 ± 0.390	3.27 ± 0.05	-0.31 ± 0.05	0.92 ± 0.07	10.05 ± 0.11	5.9	8.3	A2
HD 208313	5016 ± 60	0.780 ± 0.040	4.51 ± 0.05	0.02 ± 0.05	0.81 ± 0.04	9.87 ± 0.49	48.8	7.8	A1
HD 209393	5651 ± 60	0.860 ± 0.040	4.57 ± 0.05	-0.14 ± 0.05	0.93 ± 0.04	9.31 ± 0.34	29.4	7.9	A1
HD 210373	4876 ± 60	5.060 ± 0.600	3.15 ± 0.05	0.21 ± 0.05	1.34 ± 0.16	9.64 ± 0.17	7.2	7.5	A1
HD 211681	5710 ± 60	1.590 ± 0.200	4.10 ± 0.05	0.35 ± 0.05	1.18 ± 0.11	9.77 ± 0.13	14.2	8.1	A1
HD 215049	5109 ± 60	2.650 ± 0.350	3.63 ± 0.05	0.06 ± 0.05	1.12 ± 0.16	9.89 ± 0.23	9.3	8.3	A1
HD 216834	5058 ± 60	3.170 ± 0.350	3.40 ± 0.05	-0.23 ± 0.05	0.91 ± 0.06	10.09 ± 0.09	7.7	8.1	A1

Table A1 *continued*

Table A1 (*continued*)

Name	T_{eff} K	R_{\star} R_{\odot}	$\log g$ dex	[Fe/H] dex	M_{\star} M_{\odot}	$\log_{10}(\text{age})$	π_{\star} mas	V mag	Notes
HD 217681	4954 ± 60	3.360 ± 0.420	3.45 ± 0.05	0.24 ± 0.05	1.20 ± 0.16	9.81 ± 0.19	10.7	7.8	A1
HD 21774	5692 ± 60	1.230 ± 0.130	4.25 ± 0.05	0.20 ± 0.05	1.02 ± 0.06	9.93 ± 0.13	18.7	8.2	A1
HD 220339	4954 ± 60	0.710 ± 0.040	4.56 ± 0.05	-0.24 ± 0.05	0.75 ± 0.04	9.79 ± 0.52	52.4	7.8	A1
HD 221504	5334 ± 60	2.360 ± 0.280	3.76 ± 0.05	0.29 ± 0.05	1.23 ± 0.12	9.76 ± 0.14	11.8	8.1	A1
HD 221822	5420 ± 60	0.760 ± 0.040	4.57 ± 0.05	-0.37 ± 0.05	0.81 ± 0.04	9.59 ± 0.48	25.8	8.4	A2
HD 222038	5629 ± 60	1.220 ± 0.130	4.25 ± 0.05	0.22 ± 0.05	1.00 ± 0.06	9.98 ± 0.12	16.3	8.4	A2
HD 222986	5859 ± 60	1.040 ± 0.070	4.47 ± 0.05	0.26 ± 0.05	1.09 ± 0.05	9.26 ± 0.29	14.7	8.8	A1
HD 224619	5454 ± 60	0.840 ± 0.060	4.49 ± 0.05	-0.17 ± 0.05	0.86 ± 0.05	9.78 ± 0.46	28.7	7.5	A1
HD 22657	4792 ± 60	4.910 ± 0.680	3.11 ± 0.05	0.07 ± 0.05	1.14 ± 0.20	9.86 ± 0.26	7.8	7.8	A1
HD 234314	5566 ± 60	1.470 ± 0.180	4.09 ± 0.05	0.14 ± 0.05	1.00 ± 0.06	10.03 ± 0.10	14.2	9.3	A1
HD 23825	5588 ± 60	2.480 ± 0.300	3.74 ± 0.05	0.14 ± 0.05	1.33 ± 0.13	9.62 ± 0.13	9.1	7.9	A1
HD 238433	4936 ± 60	4.910 ± 0.730	3.13 ± 0.05	-0.00 ± 0.05	1.24 ± 0.26	9.70 ± 0.29	5.1	8.4	A1
HD 24238	4951 ± 60	0.670 ± 0.030	4.54 ± 0.05	-0.45 ± 0.05	0.69 ± 0.03	9.96 ± 0.48	47.8	7.8	A1
HD 24892	5341 ± 60	1.630 ± 0.170	3.96 ± 0.05	-0.30 ± 0.05	0.89 ± 0.05	10.08 ± 0.09	24.6	6.9	A1
HD 26007	4778 ± 60	6.500 ± 0.970	2.81 ± 0.05	-0.13 ± 0.05	0.98 ± 0.21	10.00 ± 0.27	3.9	8.4	A1
HD 26161	6033 ± 60	1.470 ± 0.160	4.15 ± 0.05	-0.01 ± 0.05	1.14 ± 0.06	9.72 ± 0.10	24.7	6.9	A1
HD 26634	4902 ± 60	4.990 ± 0.640	3.03 ± 0.05	-0.14 ± 0.05	0.96 ± 0.16	10.02 ± 0.22	5.9	8.0	A1
HD 27496	5561 ± 60	1.490 ± 0.190	4.10 ± 0.05	0.33 ± 0.05	1.06 ± 0.09	9.95 ± 0.13	11.2	8.9	A1
HD 27859	6013 ± 60	1.070 ± 0.060	4.47 ± 0.05	0.21 ± 0.05	1.12 ± 0.04	9.19 ± 0.23	22.1	7.8	A1
HD 28005	5747 ± 60	1.290 ± 0.150	4.24 ± 0.05	0.28 ± 0.05	1.08 ± 0.08	9.82 ± 0.14	33.4	6.7	A1
HD 30708	5707 ± 60	1.220 ± 0.130	4.26 ± 0.05	0.15 ± 0.05	1.01 ± 0.05	9.94 ± 0.11	33.3	6.8	A1
HD 31253	6027 ± 60	1.720 ± 0.220	4.06 ± 0.05	0.21 ± 0.05	1.28 ± 0.11	9.60 ± 0.11	17.2	7.1	A1
HD 31423	6603 ± 60	2.180 ± 0.270	3.94 ± 0.05	0.11 ± 0.05	1.57 ± 0.10	9.28 ± 0.06	15.8	6.4	A1
HD 31451	4921 ± 60	3.800 ± 0.550	3.34 ± 0.05	0.00 ± 0.05	1.15 ± 0.22	9.84 ± 0.27	8.8	8.1	A1
HD 31560	4702 ± 60	0.740 ± 0.030	4.48 ± 0.05	0.13 ± 0.05	0.76 ± 0.03	10.00 ± 0.45	38.9	8.1	A2
HD 33636	5960 ± 60	0.990 ± 0.060	4.49 ± 0.05	-0.06 ± 0.05	1.04 ± 0.04	9.27 ± 0.29	34.0	7.1	A1
HD 3404	5339 ± 60	2.170 ± 0.260	3.81 ± 0.05	0.20 ± 0.05	1.15 ± 0.12	9.84 ± 0.16	12.2	7.9	A1
HD 3458	5101 ± 60	6.880 ± 0.850	2.95 ± 0.05	0.12 ± 0.05	1.58 ± 0.16	9.39 ± 0.15	1.8	8.2	A1
HD 35112	4895 ± 60	0.760 ± 0.040	4.46 ± 0.05	-0.08 ± 0.05	0.76 ± 0.03	10.07 ± 0.37	50.2	7.7	A2
HD 3684	6163 ± 60	2.280 ± 0.280	3.90 ± 0.05	0.33 ± 0.05	1.55 ± 0.10	9.38 ± 0.09	–	7.3	A3
HD 37008	4980 ± 60	0.690 ± 0.030	4.53 ± 0.05	-0.42 ± 0.05	0.70 ± 0.03	9.99 ± 0.44	48.7	7.7	A2
HD 37124	5604 ± 60	0.760 ± 0.040	4.60 ± 0.05	-0.45 ± 0.05	0.82 ± 0.04	9.41 ± 0.42	30.1	7.7	A2
HD 37213	5447 ± 60	1.590 ± 0.170	3.98 ± 0.05	-0.40 ± 0.05	0.87 ± 0.06	10.09 ± 0.10	12.7	8.2	A1
HD 37394	5249 ± 60	0.850 ± 0.050	4.50 ± 0.05	0.15 ± 0.05	0.89 ± 0.04	9.73 ± 0.49	81.7	6.2	A2
HD 37605	5329 ± 60	1.000 ± 0.090	4.36 ± 0.05	0.27 ± 0.05	0.91 ± 0.04	10.08 ± 0.16	21.6	8.7	A1
HD 3795	5380 ± 60	1.470 ± 0.120	4.11 ± 0.05	-0.54 ± 0.05	0.83 ± 0.02	10.16 ± 0.03	39.9	6.1	A1
HD 38467	5753 ± 60	1.430 ± 0.170	4.15 ± 0.05	0.24 ± 0.05	1.09 ± 0.10	9.86 ± 0.14	13.9	8.2	A1
HD 3861	6219 ± 60	1.280 ± 0.130	4.29 ± 0.05	0.17 ± 0.05	1.21 ± 0.05	9.40 ± 0.22	30.1	6.5	A1
HD 39094	5432 ± 60	1.830 ± 0.240	3.94 ± 0.05	0.23 ± 0.05	1.10 ± 0.11	9.92 ± 0.15	15.8	7.9	A1
HD 40537	4962 ± 60	3.070 ± 0.400	3.45 ± 0.05	-0.09 ± 0.05	0.91 ± 0.17	10.12 ± 0.22	13.6	7.3	A1
HD 4203	5582 ± 60	1.560 ± 0.200	4.08 ± 0.05	0.35 ± 0.05	1.09 ± 0.11	9.91 ± 0.15	12.7	8.7	A1
HD 42807	5730 ± 60	0.930 ± 0.050	4.52 ± 0.05	0.01 ± 0.05	0.99 ± 0.04	9.33 ± 0.34	55.2	6.4	A2
HD 4313	4943 ± 60	4.530 ± 0.580	3.24 ± 0.05	0.19 ± 0.05	1.32 ± 0.17	9.66 ± 0.19	7.6	7.8	A1
HD 43162	5617 ± 60	0.890 ± 0.040	4.55 ± 0.05	0.01 ± 0.05	0.97 ± 0.04	9.33 ± 0.36	16.3	6.4	A2
HD 4395	5495 ± 60	2.690 ± 0.300	3.61 ± 0.05	-0.15 ± 0.05	1.07 ± 0.07	9.85 ± 0.10	11.0	7.7	A1
HD 44985	5984 ± 60	1.090 ± 0.100	4.36 ± 0.05	-0.02 ± 0.05	1.06 ± 0.05	9.57 ± 0.29	30.3	7.0	A1
HD 45067	5940 ± 60	2.010 ± 0.240	3.92 ± 0.05	-0.01 ± 0.05	1.22 ± 0.11	9.68 ± 0.12	30.2	5.9	A2
HD 48345	4992 ± 60	4.110 ± 0.500	3.32 ± 0.05	0.20 ± 0.05	1.32 ± 0.16	9.66 ± 0.17	8.5	7.5	A2
HD 5133	4921 ± 60	0.750 ± 0.030	4.55 ± 0.05	-0.06 ± 0.05	0.78 ± 0.04	9.75 ± 0.52	71.7	7.2	A1
HD 53927	4899 ± 60	0.700 ± 0.030	4.56 ± 0.05	-0.29 ± 0.05	0.72 ± 0.04	9.85 ± 0.51	43.4	8.3	A1

Table A1 continued

Table A1 (*continued*)

Name	T_{eff} K	R_* R_{\odot}	$\log g$ dex	[Fe/H] dex	M_* M_{\odot}	$\log_{10}(\text{age})$	π_* mas	V mag	Notes
HD 56274	5788 ± 60	0.790 ± 0.050	4.56 ± 0.05	-0.51 ± 0.05	0.84 ± 0.04	9.48 ± 0.42	30.3	7.8	A1
HD 57204	5097 ± 60	3.150 ± 0.410	3.52 ± 0.05	0.21 ± 0.05	1.23 ± 0.15	9.76 ± 0.17	12.0	8.0	A2
HD 6030	4926 ± 60	4.300 ± 0.580	3.26 ± 0.05	0.07 ± 0.05	1.26 ± 0.20	9.71 ± 0.25	5.8	7.9	A1
HD 61606	4918 ± 60	0.770 ± 0.030	4.53 ± 0.05	0.09 ± 0.05	0.81 ± 0.04	9.81 ± 0.51	71.1	7.2	A1
HD 61995	4989 ± 60	3.900 ± 0.580	3.26 ± 0.05	-0.04 ± 0.05	0.99 ± 0.22	10.00 ± 0.28	10.9	7.2	A1
HD 63754	6033 ± 60	1.950 ± 0.240	3.99 ± 0.05	0.24 ± 0.05	1.38 ± 0.10	9.54 ± 0.08	20.1	6.5	A1
HD 64413	4906 ± 60	7.800 ± 1.110	2.69 ± 0.05	-0.15 ± 0.05	1.10 ± 0.19	9.81 ± 0.22	3.0	8.2	A1
HD 66428	5670 ± 60	1.180 ± 0.120	4.29 ± 0.05	0.23 ± 0.05	1.02 ± 0.06	9.91 ± 0.15	18.7	8.3	A1
HD 68988	5866 ± 60	1.230 ± 0.140	4.29 ± 0.05	0.31 ± 0.05	1.13 ± 0.06	9.63 ± 0.21	16.7	8.2	A1
HD 69960	5600 ± 60	1.580 ± 0.200	4.06 ± 0.05	0.28 ± 0.05	1.08 ± 0.10	9.93 ± 0.14	16.0	8.0	A1
HD 72440	5599 ± 60	2.300 ± 0.300	3.75 ± 0.05	-0.01 ± 0.05	1.09 ± 0.16	9.84 ± 0.18	7.0	8.3	A1
HD 72490	4935 ± 60	4.030 ± 0.540	3.21 ± 0.05	-0.11 ± 0.05	0.93 ± 0.18	10.07 ± 0.24	8.1	7.8	A1
HD 72687	5795 ± 60	0.950 ± 0.050	4.53 ± 0.05	0.03 ± 0.05	1.02 ± 0.04	9.26 ± 0.31	22.6	8.3	A1
HD 72760	5293 ± 60	0.840 ± 0.050	4.52 ± 0.05	0.09 ± 0.05	0.89 ± 0.04	9.67 ± 0.47	47.6	7.3	A1
HD 74390	4874 ± 60	4.500 ± 0.570	3.23 ± 0.05	0.19 ± 0.05	1.26 ± 0.17	9.74 ± 0.20	7.2	8.2	A1
HD 77818	4777 ± 60	4.340 ± 0.620	3.19 ± 0.05	-0.01 ± 0.05	1.07 ± 0.19	9.95 ± 0.26	8.5	7.6	A1
HD 80367	5073 ± 60	0.830 ± 0.040	4.43 ± 0.05	0.04 ± 0.05	0.81 ± 0.03	10.08 ± 0.27	35.2	8.2	A1
HD 80606	5525 ± 60	1.130 ± 0.110	4.31 ± 0.05	0.29 ± 0.05	0.98 ± 0.05	9.98 ± 0.15	15.3	9.0	A1
HD 8407	4923 ± 60	4.920 ± 0.670	3.05 ± 0.05	-0.12 ± 0.05	0.97 ± 0.17	10.01 ± 0.23	6.3	7.8	A1
HD 84737	5872 ± 60	1.550 ± 0.190	4.10 ± 0.05	0.14 ± 0.05	1.13 ± 0.09	9.80 ± 0.12	54.3	5.1	A2
HD 8553	5054 ± 60	0.800 ± 0.040	4.48 ± 0.05	-0.01 ± 0.05	0.81 ± 0.04	10.01 ± 0.41	32.1	8.5	A1
HD 8594	4800 ± 60	5.400 ± 0.730	3.07 ± 0.05	0.14 ± 0.05	1.26 ± 0.20	9.73 ± 0.24	10.7	7.2	A2
HD 86081	5939 ± 60	1.520 ± 0.180	4.14 ± 0.05	0.23 ± 0.05	1.19 ± 0.09	9.69 ± 0.11	9.7	8.7	A1
HD 87424	5017 ± 60	0.760 ± 0.030	4.56 ± 0.05	-0.05 ± 0.05	0.81 ± 0.04	9.66 ± 0.51	43.2	8.1	A1
HD 87883	4942 ± 60	0.780 ± 0.040	4.50 ± 0.05	0.13 ± 0.05	0.81 ± 0.04	9.92 ± 0.48	55.3	7.5	A1
HD 88133	5392 ± 60	2.020 ± 0.240	3.88 ± 0.05	0.33 ± 0.05	1.18 ± 0.10	9.82 ± 0.12	13.5	8.1	A1
HD 88654	5197 ± 60	2.940 ± 0.370	3.59 ± 0.05	0.19 ± 0.05	1.24 ± 0.15	9.73 ± 0.16	9.9	7.7	A1
HD 93396	5327 ± 60	2.460 ± 0.310	3.74 ± 0.05	0.31 ± 0.05	1.25 ± 0.14	9.74 ± 0.14	8.9	8.0	A2
HD 95088	5103 ± 60	2.670 ± 0.310	3.65 ± 0.05	0.28 ± 0.05	1.19 ± 0.12	9.81 ± 0.15	9.0	8.4	A1
HD 95526	4832 ± 60	4.250 ± 0.650	3.20 ± 0.05	-0.06 ± 0.05	1.05 ± 0.22	9.96 ± 0.27	6.2	8.3	A1
HD 9625	4946 ± 60	7.260 ± 0.830	2.89 ± 0.05	0.16 ± 0.05	1.53 ± 0.14	9.46 ± 0.14	6.3	8.4	A1
HD 96612	4862 ± 60	0.730 ± 0.030	4.53 ± 0.05	-0.11 ± 0.05	0.75 ± 0.04	9.90 ± 0.50	43.9	8.3	A1
KOI-1925	5410 ± 60	0.900 ± 0.050	4.48 ± 0.03	0.11 ± 0.06	0.91 ± 0.04	9.81 ± 0.34	14.4	9.6	B1
KOI-975	6190 ± 60	1.840 ± 0.140	4.00 ± 0.03	-0.16 ± 0.06	1.26 ± 0.09	9.53 ± 0.10	9.0	8.2	B1
KOI-1612	6060 ± 60	1.190 ± 0.080	4.29 ± 0.03	-0.20 ± 0.06	1.02 ± 0.06	9.75 ± 0.11	11.0	8.8	B1
KIC 10018963	6020 ± 60	1.830 ± 0.150	3.95 ± 0.03	-0.35 ± 0.06	1.10 ± 0.10	9.72 ± 0.12	7.0	8.8	B1
KIC 10068307	6114 ± 60	2.020 ± 0.160	3.93 ± 0.03	-0.22 ± 0.06	1.30 ± 0.09	9.49 ± 0.11	8.6	8.2	B1
KIC 10162436	6200 ± 60	2.030 ± 0.150	3.95 ± 0.03	-0.08 ± 0.06	1.36 ± 0.09	9.48 ± 0.09	7.2	8.7	B1
KIC 10355856	6350 ± 60	1.640 ± 0.120	4.08 ± 0.03	-0.19 ± 0.06	1.21 ± 0.09	9.58 ± 0.10	5.6	9.2	B1
KIC 10454113	6120 ± 60	1.200 ± 0.080	4.31 ± 0.03	-0.06 ± 0.06	1.10 ± 0.06	9.60 ± 0.15	8.9	8.7	B1
KIC 10516096	5940 ± 60	1.390 ± 0.100	4.18 ± 0.03	-0.06 ± 0.06	1.08 ± 0.05	9.78 ± 0.08	7.3	9.5	B1
KIC 10644253	6030 ± 60	1.100 ± 0.060	4.40 ± 0.03	0.12 ± 0.06	1.12 ± 0.04	9.34 ± 0.26	10.1	9.3	B1
KIC 10709834	6508 ± 60	1.720 ± 0.130	4.09 ± 0.03	-0.08 ± 0.06	1.34 ± 0.08	9.42 ± 0.07	4.3	9.8	B1
KIC 11026764	5682 ± 60	2.060 ± 0.190	3.88 ± 0.03	0.05 ± 0.06	1.20 ± 0.14	9.74 ± 0.16	–	9.7	B3
KIC 11137075	5590 ± 60	1.630 ± 0.120	4.01 ± 0.03	-0.06 ± 0.06	1.00 ± 0.06	9.98 ± 0.10	3.8	10.9	B1
KIC 11244118	5745 ± 60	1.620 ± 0.140	4.09 ± 0.03	0.35 ± 0.06	1.20 ± 0.10	9.74 ± 0.13	6.3	9.8	B1
KIC 11414712	5635 ± 60	2.180 ± 0.180	3.80 ± 0.03	-0.05 ± 0.06	1.08 ± 0.13	9.85 ± 0.15	7.8	8.7	B1
KIC 11717120	5150 ± 60	2.230 ± 0.140	3.68 ± 0.03	-0.30 ± 0.06	0.86 ± 0.04	10.13 ± 0.06	6.8	9.5	B1
KIC 12009504	6065 ± 60	1.350 ± 0.110	4.21 ± 0.03	-0.09 ± 0.06	1.10 ± 0.07	9.71 ± 0.09	7.0	9.3	B1
KIC 12258514	5990 ± 60	1.550 ± 0.110	4.11 ± 0.03	0.04 ± 0.06	1.14 ± 0.07	9.75 ± 0.10	12.1	8.2	B1

Table A1 *continued*

Table A1 (*continued*)

Name	T_{eff} K	R_{\star} R_{\odot}	$\log g$ dex	[Fe/H] dex	M_{\star} M_{\odot}	$\log_{10}(\text{age})$	π_{\star} mas	V mag	Notes
KIC 1435467	6264 ± 60	1.690 ± 0.130	4.09 ± 0.03	-0.01 ± 0.06	1.30 ± 0.08	9.51 ± 0.09	5.6	9.0	B1
KIC 3427720	6040 ± 60	1.100 ± 0.070	4.38 ± 0.03	-0.03 ± 0.06	1.08 ± 0.05	9.50 ± 0.25	10.5	9.2	B1
KIC 3656476	5710 ± 60	1.320 ± 0.100	4.23 ± 0.03	0.34 ± 0.06	1.10 ± 0.08	9.81 ± 0.14	8.6	9.6	B1
KIC 4914923	5905 ± 60	1.370 ± 0.100	4.21 ± 0.03	0.17 ± 0.06	1.12 ± 0.07	9.76 ± 0.11	7.3	9.5	B1
KIC 5021689	6168 ± 60	1.810 ± 0.140	4.02 ± 0.03	-0.08 ± 0.06	1.28 ± 0.09	9.54 ± 0.10	–	–	B3
KIC 5184732	5840 ± 60	1.310 ± 0.100	4.26 ± 0.03	0.38 ± 0.06	1.16 ± 0.06	9.65 ± 0.13	14.2	8.3	B1
KIC 5596656	5094 ± 60	3.320 ± 0.270	3.35 ± 0.03	-0.46 ± 0.06	0.90 ± 0.08	10.07 ± 0.14	3.0	9.8	B1
KIC 5773345	6130 ± 60	1.940 ± 0.150	4.00 ± 0.03	0.21 ± 0.06	1.39 ± 0.09	9.51 ± 0.08	5.2	9.3	B1
KIC 5955122	5837 ± 60	2.090 ± 0.150	3.87 ± 0.03	-0.17 ± 0.06	1.18 ± 0.08	9.65 ± 0.12	5.2	9.4	B1
KIC 6106415	5990 ± 60	1.170 ± 0.080	4.31 ± 0.03	-0.09 ± 0.06	1.04 ± 0.06	9.73 ± 0.11	24.1	7.2	B1
KIC 6116048	5935 ± 60	1.170 ± 0.080	4.28 ± 0.03	-0.24 ± 0.06	0.96 ± 0.05	9.87 ± 0.09	13.3	8.5	B1
KIC 6225718	6230 ± 60	1.190 ± 0.070	4.32 ± 0.03	-0.17 ± 0.06	1.09 ± 0.06	9.56 ± 0.16	19.1	7.5	B1
KIC 6442183	5760 ± 60	1.650 ± 0.110	4.03 ± 0.03	-0.11 ± 0.06	1.07 ± 0.05	9.81 ± 0.10	10.9	8.6	B1
KIC 6603624	5625 ± 60	1.150 ± 0.080	4.32 ± 0.03	0.28 ± 0.06	1.01 ± 0.06	9.90 ± 0.14	12.0	9.2	B1
KIC 6933899	5860 ± 60	1.550 ± 0.110	4.09 ± 0.03	0.02 ± 0.06	1.09 ± 0.06	9.85 ± 0.09	7.0	9.8	B1
KIC 7206837	6304 ± 60	1.540 ± 0.110	4.17 ± 0.03	0.14 ± 0.06	1.29 ± 0.05	9.48 ± 0.07	4.8	9.8	B1
KIC 7680114	5855 ± 60	1.390 ± 0.100	4.18 ± 0.03	0.11 ± 0.06	1.08 ± 0.07	9.85 ± 0.11	5.9	10.2	B1
KIC 7747078	5840 ± 60	1.990 ± 0.150	3.91 ± 0.03	-0.26 ± 0.06	1.17 ± 0.10	9.63 ± 0.12	5.4	9.5	B1
KIC 7799349	5115 ± 60	2.670 ± 0.210	3.67 ± 0.03	0.41 ± 0.06	1.22 ± 0.12	9.78 ± 0.14	5.3	9.7	B1
KIC 7871531	5400 ± 60	0.840 ± 0.050	4.49 ± 0.03	-0.24 ± 0.06	0.82 ± 0.05	9.96 ± 0.22	15.2	9.4	B1
KIC 7940546	6264 ± 60	1.850 ± 0.150	3.99 ± 0.03	-0.19 ± 0.06	1.24 ± 0.10	9.55 ± 0.10	11.1	7.4	B1
KIC 7970740	5290 ± 60	0.720 ± 0.030	4.58 ± 0.03	-0.49 ± 0.06	0.74 ± 0.04	9.83 ± 0.48	36.6	8.0	B1
KIC 7976303	6053 ± 60	1.950 ± 0.160	3.87 ± 0.03	-0.53 ± 0.06	1.03 ± 0.09	9.81 ± 0.13	6.4	9.2	B1
KIC 8006161	5390 ± 60	0.920 ± 0.040	4.49 ± 0.03	0.34 ± 0.06	0.97 ± 0.04	9.56 ± 0.39	36.8	7.5	B1
KIC 8179536	6344 ± 60	1.330 ± 0.090	4.27 ± 0.03	0.01 ± 0.06	1.22 ± 0.05	9.41 ± 0.14	7.1	9.5	B1
KIC 8228742	6042 ± 60	1.770 ± 0.130	4.02 ± 0.03	-0.14 ± 0.06	1.19 ± 0.07	9.63 ± 0.10	5.6	9.5	B1
KIC 8394589	6114 ± 60	1.120 ± 0.070	4.32 ± 0.03	-0.36 ± 0.06	0.97 ± 0.05	9.79 ± 0.11	7.8	9.6	B1
KIC 8524425	5634 ± 60	1.800 ± 0.160	3.98 ± 0.03	0.14 ± 0.06	1.13 ± 0.11	9.85 ± 0.14	5.6	9.9	B1
KIC 8561221	5245 ± 60	2.560 ± 0.270	3.61 ± 0.03	-0.06 ± 0.06	0.96 ± 0.18	10.04 ± 0.24	3.5	10.1	B1
KIC 8694723	6120 ± 60	1.420 ± 0.100	4.10 ± 0.03	-0.59 ± 0.06	0.93 ± 0.04	9.93 ± 0.06	8.2	8.9	B1
KIC 8702606	5540 ± 60	2.240 ± 0.180	3.76 ± 0.03	-0.09 ± 0.06	1.05 ± 0.12	9.90 ± 0.14	5.4	9.5	B1
KIC 8751420	5264 ± 60	2.270 ± 0.160	3.70 ± 0.03	-0.15 ± 0.06	0.94 ± 0.06	10.07 ± 0.10	17.2	7.0	B1
KIC 8938364	5630 ± 60	1.330 ± 0.100	4.16 ± 0.03	-0.20 ± 0.06	0.94 ± 0.06	9.97 ± 0.10	6.2	10.2	B1
KIC 9098294	5840 ± 60	1.140 ± 0.080	4.30 ± 0.03	-0.13 ± 0.06	0.98 ± 0.05	9.87 ± 0.09	8.0	9.9	B1
KIC 9139151	6125 ± 60	1.140 ± 0.060	4.38 ± 0.03	0.11 ± 0.06	1.15 ± 0.04	9.29 ± 0.24	9.6	9.3	B1
KIC 9139163	6400 ± 60	1.530 ± 0.110	4.18 ± 0.03	0.15 ± 0.06	1.32 ± 0.05	9.41 ± 0.08	9.6	8.3	B1
KIC 9206432	6608 ± 60	1.490 ± 0.090	4.23 ± 0.03	0.23 ± 0.06	1.39 ± 0.06	9.16 ± 0.13	6.6	9.1	B1
HIP 10337	4051 ± 239	0.694 ± 0.072	4.67 ± 0.06	0.12 ± 0.10	0.65 ± 0.07	9.60 ± 0.53	42.6	9.8	C1
HIP 105341	4033 ± 242	0.673 ± 0.063	4.67 ± 0.05	-0.05 ± 0.10	0.64 ± 0.07	9.64 ± 0.52	63.2	9.1	C1
HIP 114156	4146 ± 209	0.660 ± 0.051	4.67 ± 0.05	-0.02 ± 0.10	0.65 ± 0.06	9.59 ± 0.52	45.1	9.6	C1
HIP 118261	4615 ± 214	0.715 ± 0.051	4.62 ± 0.05	-0.04 ± 0.10	0.74 ± 0.06	9.58 ± 0.52	44.0	8.7	C1
HIP 12493	4276 ± 193	0.662 ± 0.047	4.68 ± 0.04	-0.29 ± 0.10	0.64 ± 0.06	9.60 ± 0.52	41.9	9.5	C1
HIP 15095	4227 ± 199	0.653 ± 0.047	4.67 ± 0.04	-0.21 ± 0.10	0.64 ± 0.06	9.61 ± 0.52	54.0	9.1	C1
HIP 1532	4039 ± 241	0.594 ± 0.055	4.71 ± 0.06	-0.37 ± 0.10	0.58 ± 0.06	9.60 ± 0.53	49.3	9.9	C1
HIP 19165	4298 ± 200	0.659 ± 0.047	4.68 ± 0.04	-0.22 ± 0.10	0.65 ± 0.06	9.56 ± 0.52	38.7	9.7	C1
HIP 25220	4505 ± 179	0.702 ± 0.042	4.63 ± 0.04	0.05 ± 0.10	0.73 ± 0.06	9.58 ± 0.52	68.5	7.9	C1
HIP 36551	4395 ± 193	0.669 ± 0.046	4.66 ± 0.04	-0.30 ± 0.10	0.66 ± 0.06	9.63 ± 0.52	48.5	8.9	C1
HIP 40375	4334 ± 209	0.711 ± 0.052	4.65 ± 0.04	0.03 ± 0.10	0.70 ± 0.06	9.55 ± 0.52	52.0	8.8	C1
HIP 40910	4159 ± 228	0.633 ± 0.053	4.67 ± 0.05	-0.06 ± 0.10	0.64 ± 0.06	9.60 ± 0.52	44.4	9.7	C1
HIP 45839	4426 ± 198	0.714 ± 0.050	4.63 ± 0.04	0.05 ± 0.10	0.72 ± 0.06	9.61 ± 0.52	41.8	9.1	C1

Table A1 continued

Table A1 (*continued*)

Name	T_{eff} K	R_* R_{\odot}	$\log g$ dex	[Fe/H] dex	M_* M_{\odot}	$\log_{10}(\text{age})$	π_* mas	V mag	Notes
HIP 47201	4207 ± 212	0.696 ± 0.054	4.66 ± 0.05	0.03 ± 0.10	0.67 ± 0.06	9.63 ± 0.52	44.5	9.4	C1
HIP 48411	4357 ± 199	0.742 ± 0.072	4.63 ± 0.04	0.20 ± 0.10	0.72 ± 0.07	9.62 ± 0.52	47.7	8.8	C2
HIP 4845	3967 ± 301	0.632 ± 0.073	4.72 ± 0.12	-0.19 ± 0.10	0.59 ± 0.09	9.62 ± 0.52	46.7	10.0	C1
HIP 54810	4395 ± 185	0.681 ± 0.044	4.64 ± 0.04	0.03 ± 0.10	0.70 ± 0.06	9.58 ± 0.52	54.2	8.6	C1
HIP 5663	4186 ± 222	0.672 ± 0.055	4.67 ± 0.05	-0.05 ± 0.10	0.66 ± 0.06	9.58 ± 0.52	44.0	9.5	C1
HIP 66222	3904 ± 266	0.667 ± 0.087	4.70 ± 0.07	-0.11 ± 0.10	0.59 ± 0.08	9.62 ± 0.52	48.8	9.9	C2
HIP 93871	4449 ± 177	0.681 ± 0.043	4.67 ± 0.04	-0.47 ± 0.10	0.65 ± 0.05	9.67 ± 0.52	40.8	9.2	C1
HIP 97051	4200 ± 248	0.631 ± 0.057	4.70 ± 0.07	-0.19 ± 0.10	0.62 ± 0.07	9.59 ± 0.52	38.5	10.0	C1
HD 111631	3989 ± 60	0.646 ± 0.020	4.66 ± 0.05	0.24 ± 0.08	0.70 ± 0.07	9.79 ± 0.51	93.7	8.5	D1
HD 1326B	3218 ± 60	0.192 ± 0.008	5.07 ± 0.05	-0.30 ± 0.08	0.16 ± 0.02	9.64 ± 0.53	–	11.0	D3
HD 157881	4124 ± 60	0.649 ± 0.020	4.66 ± 0.05	0.19 ± 0.08	0.71 ± 0.07	9.65 ± 0.52	129.3	7.6	D1
HD 165222	3614 ± 60	0.459 ± 0.016	4.79 ± 0.05	-0.22 ± 0.08	0.47 ± 0.05	9.70 ± 0.52	128.3	9.4	D2
HD 180617	3558 ± 60	0.474 ± 0.016	4.76 ± 0.05	0.10 ± 0.08	0.47 ± 0.05	9.70 ± 0.52	169.4	9.1	D1
HD 209290	3848 ± 60	0.546 ± 0.019	4.74 ± 0.05	0.02 ± 0.08	0.59 ± 0.06	9.56 ± 0.52	94.2	9.1	D1
HD 232979	3929 ± 60	0.608 ± 0.020	4.68 ± 0.05	-0.11 ± 0.08	0.65 ± 0.07	9.78 ± 0.51	101.2	8.9	D1
HD 245409	3966 ± 60	0.601 ± 0.020	4.69 ± 0.05	0.05 ± 0.08	0.65 ± 0.07	9.66 ± 0.52	87.7	8.9	D1
HD 265866	3448 ± 60	0.358 ± 0.013	4.88 ± 0.05	-0.02 ± 0.08	0.35 ± 0.04	9.66 ± 0.52	180.3	10.1	D1
HD 28343	4124 ± 62	0.687 ± 0.023	4.64 ± 0.05	0.39 ± 0.08	0.74 ± 0.07	9.77 ± 0.51	89.0	8.3	D1
GJ 628	3272 ± 60	0.325 ± 0.012	4.88 ± 0.05	-0.03 ± 0.08	0.29 ± 0.03	9.85 ± 0.48	232.3	10.1	D1
GL 105B	3284 ± 60	0.278 ± 0.010	4.94 ± 0.05	-0.12 ± 0.03	0.25 ± 0.03	9.85 ± 0.51	–	11.7	D3
GL 109	3405 ± 60	0.364 ± 0.014	4.85 ± 0.05	-0.10 ± 0.08	0.34 ± 0.03	9.72 ± 0.51	132.4	10.6	D2
GL 2066	3500 ± 60	0.461 ± 0.017	4.77 ± 0.05	-0.12 ± 0.08	0.45 ± 0.04	9.78 ± 0.51	112.0	10.1	D1
GL 239	3801 ± 60	0.423 ± 0.015	4.86 ± 0.05	-0.34 ± 0.08	0.47 ± 0.05	9.49 ± 0.52	99.5	9.6	D1
GL 250B	3481 ± 60	0.460 ± 0.017	4.76 ± 0.05	0.14 ± 0.03	0.44 ± 0.04	9.69 ± 0.52	–	10.1	D3
GL 273	3317 ± 60	0.315 ± 0.012	4.89 ± 0.05	-0.11 ± 0.08	0.28 ± 0.03	9.85 ± 0.49	263.3	9.9	D2
GL 382	3623 ± 60	0.522 ± 0.019	4.72 ± 0.05	0.13 ± 0.08	0.53 ± 0.05	9.75 ± 0.52	128.0	9.3	D2
GL 393	3548 ± 60	0.420 ± 0.016	4.82 ± 0.05	-0.18 ± 0.08	0.43 ± 0.04	9.66 ± 0.52	138.3	9.7	D2
GL 514	3727 ± 61	0.483 ± 0.016	4.79 ± 0.05	-0.09 ± 0.08	0.53 ± 0.05	9.54 ± 0.52	131.1	9.0	D2
GL 625	3475 ± 60	0.331 ± 0.012	4.90 ± 0.05	-0.35 ± 0.08	0.32 ± 0.03	9.75 ± 0.51	154.1	10.2	D1
GL 686	3657 ± 60	0.424 ± 0.015	4.83 ± 0.05	-0.25 ± 0.08	0.44 ± 0.04	9.63 ± 0.53	123.0	9.6	D2
GL 694	3464 ± 61	0.440 ± 0.017	4.79 ± 0.05	0.00 ± 0.08	0.43 ± 0.04	9.72 ± 0.52	105.4	10.5	D2
GL 745A	3500 ± 60	0.310 ± 0.012	4.93 ± 0.05	-0.33 ± 0.08	0.30 ± 0.03	9.75 ± 0.52	113.4	10.8	D1
GL 806	3542 ± 61	0.443 ± 0.018	4.78 ± 0.05	-0.15 ± 0.08	0.43 ± 0.04	9.72 ± 0.52	83.0	10.7	D1
GL 83.1	3080 ± 60	0.187 ± 0.010	5.05 ± 0.05	-0.16 ± 0.08	0.14 ± 0.01	9.68 ± 0.53	–	12.3	D3
GL 87	3638 ± 62	0.443 ± 0.017	4.79 ± 0.05	-0.36 ± 0.08	0.44 ± 0.04	9.74 ± 0.52	94.8	10.0	D1
GL 875	3740 ± 61	0.563 ± 0.024	4.70 ± 0.05	0.02 ± 0.08	0.58 ± 0.06	9.77 ± 0.51	71.4	9.8	D2
GL 896A	3353 ± 60	0.409 ± 0.016	4.79 ± 0.05	0.03 ± 0.08	0.38 ± 0.04	9.76 ± 0.51	–	10.2	D3
GL 908	3646 ± 60	0.407 ± 0.014	4.83 ± 0.05	-0.45 ± 0.08	0.41 ± 0.04	9.72 ± 0.52	169.1	9.0	D1
HIP 104432	3545 ± 60	0.369 ± 0.016	4.86 ± 0.05	-0.45 ± 0.08	0.36 ± 0.04	9.70 ± 0.52	84.9	10.9	D1
HIP 109388	3530 ± 60	0.470 ± 0.018	4.78 ± 0.05	0.37 ± 0.08	0.48 ± 0.05	9.65 ± 0.52	113.2	10.4	D1
HIP 11048	3785 ± 62	0.599 ± 0.021	4.67 ± 0.05	0.14 ± 0.08	0.61 ± 0.06	9.85 ± 0.49	83.9	9.3	D2
HIP 115332	3324 ± 60	0.416 ± 0.020	4.79 ± 0.05	0.24 ± 0.08	0.39 ± 0.04	9.68 ± 0.52	93.5	11.7	D2
HIP 115562	3764 ± 60	0.539 ± 0.020	4.74 ± 0.05	0.31 ± 0.08	0.58 ± 0.06	9.55 ± 0.52	75.8	10.1	D1
HIP 15366	3700 ± 61	0.628 ± 0.031	4.65 ± 0.05	0.53 ± 0.08	0.64 ± 0.06	9.76 ± 0.51	57.8	10.3	D2
HIP 1734	3600 ± 60	0.528 ± 0.028	4.73 ± 0.05	0.27 ± 0.08	0.55 ± 0.06	9.69 ± 0.52	55.2	11.1	D1
HIP 21556	3671 ± 61	0.444 ± 0.017	4.82 ± 0.05	-0.04 ± 0.08	0.47 ± 0.05	9.55 ± 0.52	89.5	10.3	D1
HIP 22762	3506 ± 60	0.421 ± 0.019	4.81 ± 0.05	-0.24 ± 0.08	0.41 ± 0.04	9.75 ± 0.51	83.7	10.9	D1
HIP 23512	3365 ± 60	0.284 ± 0.013	4.95 ± 0.05	-0.12 ± 0.08	0.26 ± 0.03	9.75 ± 0.52	107.9	11.7	D1
HIP 36338	3448 ± 60	0.404 ± 0.019	4.82 ± 0.05	-0.01 ± 0.08	0.40 ± 0.04	9.69 ± 0.51	79.7	11.5	D2
HIP 36834	3681 ± 60	0.385 ± 0.016	4.87 ± 0.05	-0.37 ± 0.08	0.40 ± 0.04	9.62 ± 0.52	85.2	10.4	D1

Table A1 continued

Table A1 (*continued*)

Name	T_{eff} K	R_* R_{\odot}	$\log g$ dex	[Fe/H] dex	M_* M_{\odot}	$\log_{10}(\text{age})$	π_* mas	V mag	Notes
HIP 37217	3358 ± 60	0.315 ± 0.016	4.90 ± 0.05	-0.18 ± 0.08	0.29 ± 0.03	9.81 ± 0.51	92.2	11.7	D2
HIP 46769	3692 ± 60	0.518 ± 0.021	4.74 ± 0.05	-0.20 ± 0.08	0.53 ± 0.05	9.72 ± 0.52	73.6	10.1	D1
HIP 47513	3500 ± 60	0.485 ± 0.019	4.74 ± 0.05	-0.05 ± 0.08	0.47 ± 0.05	9.83 ± 0.49	86.2	10.4	D1
HIP 51007	3700 ± 60	0.497 ± 0.020	4.76 ± 0.05	-0.02 ± 0.08	0.52 ± 0.05	9.63 ± 0.53	78.3	10.1	D1
HIP 5643	3056 ± 60	0.168 ± 0.009	5.10 ± 0.05	-0.26 ± 0.08	0.13 ± 0.01	9.61 ± 0.52	269.1	12.1	D2
HIP 57050	3304 ± 61	0.376 ± 0.018	4.81 ± 0.05	0.07 ± 0.08	0.34 ± 0.03	9.78 ± 0.51	90.9	12.0	D1
HIP 57548	3192 ± 60	0.197 ± 0.008	5.08 ± 0.05	-0.02 ± 0.08	0.17 ± 0.02	9.62 ± 0.53	295.8	11.2	D1
HIP 59748	3900 ± 61	0.669 ± 0.038	4.63 ± 0.06	0.14 ± 0.08	0.70 ± 0.07	9.84 ± 0.51	43.8	10.5	D1
HIP 60093	3993 ± 60	0.643 ± 0.037	4.67 ± 0.06	0.46 ± 0.08	0.70 ± 0.07	9.58 ± 0.52	42.2	10.6	D1
HIP 61706	3463 ± 60	0.466 ± 0.025	4.77 ± 0.06	0.26 ± 0.08	0.47 ± 0.05	9.64 ± 0.53	65.0	11.5	D2
HIP 65016	3650 ± 60	0.598 ± 0.025	4.66 ± 0.05	0.40 ± 0.08	0.60 ± 0.06	9.87 ± 0.50	58.9	10.6	D1
HIP 71253	3211 ± 60	0.310 ± 0.013	4.89 ± 0.05	0.17 ± 0.08	0.27 ± 0.03	9.89 ± 0.49	159.1	11.3	D1
HIP 8051	3458 ± 60	0.414 ± 0.017	4.81 ± 0.05	-0.13 ± 0.08	0.40 ± 0.04	9.76 ± 0.51	89.2	10.9	D1
HIP 91699	3400 ± 61	0.394 ± 0.019	4.81 ± 0.05	-0.16 ± 0.08	0.37 ± 0.04	9.75 ± 0.51	92.8	11.3	D1
HD 101501	5309 ± 27	0.940 ± 0.010	4.42 ± 0.02	-0.03 ± 0.10	0.84 ± 0.03	10.14 ± 0.05	104.8	5.3	E2
HD 10476	5242 ± 12	0.810 ± 0.004	4.57 ± 0.02	-0.02 ± 0.10	0.88 ± 0.04	9.51 ± 0.42	133.9	5.2	E2
HD 10697	5442 ± 65	1.915 ± 0.052	3.91 ± 0.05	0.12 ± 0.10	1.09 ± 0.10	9.92 ± 0.12	30.7	6.3	E2
HD 10700	5290 ± 39	0.815 ± 0.012	4.50 ± 0.03	-0.48 ± 0.10	0.76 ± 0.04	10.09 ± 0.16	274.2	3.5	E2
HD 107383	4705 ± 24	15.781 ± 0.344	2.15 ± 0.04	-0.30 ± 0.10	1.29 ± 0.10	9.56 ± 0.09	9.0	4.7	E2
HD 10780	5398 ± 75	0.819 ± 0.024	4.56 ± 0.03	0.03 ± 0.10	0.90 ± 0.04	9.36 ± 0.39	100.2	5.6	E2
HD 115617	5538 ± 13	0.987 ± 0.005	4.41 ± 0.02	0.01 ± 0.10	0.92 ± 0.04	9.97 ± 0.07	117.3	4.7	E2
HD 117176	5406 ± 64	1.968 ± 0.047	3.84 ± 0.05	-0.06 ± 0.10	0.97 ± 0.10	10.02 ± 0.13	54.7	5.0	E1
HD 11964A	5013 ± 62	2.143 ± 0.069	3.77 ± 0.05	0.14 ± 0.10	0.99 ± 0.07	10.09 ± 0.10	29.4	6.4	E2
HD 119850	3618 ± 31	0.484 ± 0.008	4.78 ± 0.02	-0.30 ± 0.10	0.50 ± 0.02	9.84 ± 0.49	184.1	8.5	E2
HD 120136	6620 ± 67	1.331 ± 0.027	4.30 ± 0.02	0.24 ± 0.10	1.31 ± 0.03	9.07 ± 0.11	64.1	4.5	E2
HD 126660	6211 ± 19	1.734 ± 0.011	4.08 ± 0.02	-0.02 ± 0.10	1.31 ± 0.05	9.53 ± 0.06	68.6	4.0	E2
HD 130948	5787 ± 57	1.112 ± 0.023	4.35 ± 0.04	-0.05 ± 0.10	0.99 ± 0.05	9.86 ± 0.13	55.7	5.9	E2
HD 131156	5483 ± 32	0.863 ± 0.011	4.53 ± 0.03	-0.14 ± 0.10	0.91 ± 0.05	9.62 ± 0.40	149.3	4.6	E2
HD 1326	3567 ± 11	0.386 ± 0.002	4.87 ± 0.01	-0.36 ± 0.10	0.40 ± 0.01	9.66 ± 0.52	280.7	8.1	E1
HD 136202	5661 ± 87	2.143 ± 0.067	3.83 ± 0.06	-0.04 ± 0.10	1.11 ± 0.13	9.82 ± 0.16	40.5	5.1	E2
HD 143761	5627 ± 54	1.362 ± 0.026	4.15 ± 0.03	-0.22 ± 0.10	0.96 ± 0.06	9.96 ± 0.10	57.4	5.4	E2
HD 145675	5518 ± 102	0.867 ± 0.032	4.53 ± 0.03	0.44 ± 0.10	0.98 ± 0.04	9.27 ± 0.36	55.9	6.7	E1
HD 1461	5386 ± 60	1.244 ± 0.030	4.22 ± 0.04	0.16 ± 0.10	0.93 ± 0.03	10.15 ± 0.05	42.7	6.5	E2
HD 149661	5337 ± 41	0.759 ± 0.012	4.59 ± 0.01	0.04 ± 0.10	0.85 ± 0.03	9.22 ± 0.29	102.3	5.8	E2
HD 157214	5738 ± 48	1.116 ± 0.019	4.29 ± 0.04	-0.37 ± 0.10	0.87 ± 0.06	10.04 ± 0.11	69.5	5.4	E2
HD 158633	5203 ± 46	0.789 ± 0.014	4.54 ± 0.04	-0.41 ± 0.10	0.77 ± 0.05	10.03 ± 0.33	78.3	6.4	E1
HD 16160	4662 ± 17	0.795 ± 0.006	4.54 ± 0.01	-0.08 ± 0.10	0.77 ± 0.01	10.16 ± 0.04	138.7	5.8	E2
HD 161797	5502 ± 55	1.745 ± 0.035	3.99 ± 0.03	0.23 ± 0.10	1.08 ± 0.05	9.93 ± 0.07	119.0	3.4	E2
HD 164259	6454 ± 113	1.961 ± 0.071	4.01 ± 0.04	-0.03 ± 0.10	1.43 ± 0.07	9.40 ± 0.08	43.1	4.6	E2
HD 166	5327 ± 39	0.917 ± 0.009	4.45 ± 0.03	0.08 ± 0.10	0.87 ± 0.04	10.05 ± 0.13	72.6	6.1	E1
HD 16765	6356 ± 46	1.208 ± 0.029	4.35 ± 0.04	-0.15 ± 0.10	1.17 ± 0.06	9.32 ± 0.25	46.2	5.7	E2
HD 168151	6221 ± 39	1.758 ± 0.022	4.03 ± 0.04	-0.28 ± 0.10	1.19 ± 0.10	9.60 ± 0.11	42.6	5.0	E2
HD 16895	6153 ± 25	1.319 ± 0.011	4.26 ± 0.02	0.00 ± 0.10	1.16 ± 0.05	9.59 ± 0.09	89.0	4.1	E2
HD 173667	6296 ± 19	2.064 ± 0.017	3.96 ± 0.01	-0.03 ± 0.10	1.43 ± 0.04	9.44 ± 0.03	52.4	4.2	E2
HD 173701	5297 ± 53	0.952 ± 0.021	4.43 ± 0.04	0.24 ± 0.10	0.88 ± 0.05	10.06 ± 0.18	36.8	7.5	E1
HD 173739	3407 ± 15	0.356 ± 0.004	4.90 ± 0.01	-0.49 ± 0.10	0.36 ± 0.01	9.83 ± 0.48	283.5	8.9	E1
HD 173740	3104 ± 28	0.323 ± 0.006	4.92 ± 0.01	-0.36 ± 0.10	0.30 ± 0.01	10.01 ± 0.36	286.4	9.7	E1
HD 177153	5909 ± 69	1.289 ± 0.037	4.25 ± 0.04	-0.06 ± 0.10	1.06 ± 0.05	9.80 ± 0.10	24.1	7.2	E1
HD 181420	6283 ± 106	1.730 ± 0.084	4.09 ± 0.06	-0.03 ± 0.10	1.31 ± 0.09	9.50 ± 0.12	20.0	6.5	E1
HD 182572	5643 ± 84	1.379 ± 0.042	4.19 ± 0.05	0.34 ± 0.10	1.06 ± 0.09	9.92 ± 0.17	66.0	5.2	E2

Table A1 continued

Table A1 (*continued*)

Name	T_{eff} K	R_* R_{\odot}	$\log g$ dex	[Fe/H] dex	M_* M_{\odot}	$\log_{10}(\text{age})$	π_* mas	V mag	Notes
HD 182736	5239 ± 37	2.703 ± 0.071	3.57 ± 0.08	-0.06 ± 0.10	0.97 ± 0.17	10.02 ± 0.22	17.2	7.0	E1
HD 185144	5246 ± 26	0.778 ± 0.008	4.58 ± 0.03	-0.19 ± 0.10	0.84 ± 0.05	9.51 ± 0.43	173.6	4.7	E1
HD 186408	5760 ± 57	1.255 ± 0.026	4.25 ± 0.03	0.05 ± 0.10	1.02 ± 0.05	9.92 ± 0.10	47.0	6.0	E1
HD 186427	5678 ± 66	1.169 ± 0.027	4.30 ± 0.04	0.04 ± 0.10	0.97 ± 0.05	9.97 ± 0.11	47.1	6.2	E1
HD 187637	6155 ± 85	1.306 ± 0.047	4.27 ± 0.06	-0.09 ± 0.10	1.13 ± 0.07	9.61 ± 0.17	19.1	7.5	E1
HD 188512	4920 ± 102	3.210 ± 0.133	3.39 ± 0.09	-0.14 ± 0.10	0.92 ± 0.15	10.11 ± 0.17	73.0	3.7	E2
HD 190360	5461 ± 75	1.200 ± 0.033	4.26 ± 0.04	0.21 ± 0.10	0.94 ± 0.05	10.11 ± 0.09	62.4	5.7	E1
HD 190406	5763 ± 49	1.115 ± 0.021	4.34 ± 0.03	0.03 ± 0.10	1.00 ± 0.04	9.87 ± 0.11	58.0	5.8	E1
HD 19373	5832 ± 33	1.415 ± 0.015	4.17 ± 0.02	0.08 ± 0.10	1.07 ± 0.05	9.88 ± 0.09	94.9	4.0	E2
HD 195564	5421 ± 118	1.867 ± 0.083	3.91 ± 0.07	0.06 ± 0.10	1.03 ± 0.11	9.98 ± 0.15	41.3	5.7	E2
HD 199305	3692 ± 22	0.547 ± 0.007	4.72 ± 0.01	-0.21 ± 0.10	0.54 ± 0.01	10.09 ± 0.21	142.2	8.6	E1
HD 19994	5916 ± 98	1.930 ± 0.067	3.99 ± 0.05	0.17 ± 0.10	1.30 ± 0.10	9.62 ± 0.11	44.7	5.1	E2
HD 201091	4361 ± 17	0.661 ± 0.005	4.63 ± 0.02	-0.19 ± 0.10	0.68 ± 0.03	9.90 ± 0.46	287.1	5.2	E2
HD 201092	3932 ± 25	0.601 ± 0.007	4.67 ± 0.01	-0.29 ± 0.10	0.60 ± 0.01	10.09 ± 0.21	285.4	6.0	E2
HD 206860	5860 ± 83	1.019 ± 0.029	4.43 ± 0.05	-0.16 ± 0.10	1.00 ± 0.08	9.64 ± 0.37	54.4	6.0	E2
HD 21019	5261 ± 65	2.421 ± 0.076	3.64 ± 0.05	-0.41 ± 0.10	0.93 ± 0.07	10.01 ± 0.11	27.1	6.2	E2
HD 210702	4780 ± 18	5.231 ± 0.117	3.05 ± 0.09	0.03 ± 0.10	1.12 ± 0.21	9.86 ± 0.27	17.9	5.9	E2
HD 216899	3713 ± 11	0.548 ± 0.005	4.72 ± 0.01	0.06 ± 0.10	0.56 ± 0.01	9.99 ± 0.39	146.0	8.6	E1
HD 217014	5706 ± 95	1.168 ± 0.042	4.32 ± 0.06	0.17 ± 0.10	1.01 ± 0.07	9.89 ± 0.21	65.1	5.5	E2
HD 217107	5391 ± 40	1.210 ± 0.019	4.25 ± 0.03	0.31 ± 0.10	0.94 ± 0.03	10.13 ± 0.06	50.0	6.2	E1
HD 217987	3676 ± 35	0.471 ± 0.009	4.79 ± 0.02	-0.19 ± 0.10	0.49 ± 0.02	9.66 ± 0.53	303.9	7.3	E2
HD 219134	4699 ± 16	0.778 ± 0.005	4.55 ± 0.01	0.07 ± 0.10	0.77 ± 0.02	10.12 ± 0.11	153.2	5.6	E2
HD 219623	6285 ± 94	1.195 ± 0.036	4.36 ± 0.04	0.04 ± 0.10	1.18 ± 0.06	9.25 ± 0.25	49.3	5.6	E2
HD 222368	6192 ± 26	1.595 ± 0.014	4.12 ± 0.02	-0.14 ± 0.10	1.22 ± 0.06	9.60 ± 0.07	72.5	4.1	E2
HD 22484	5998 ± 39	1.622 ± 0.024	4.08 ± 0.02	-0.09 ± 0.10	1.15 ± 0.04	9.71 ± 0.09	72.9	4.3	E2
HD 23249	4955 ± 30	2.327 ± 0.029	3.70 ± 0.03	0.12 ± 0.10	0.98 ± 0.06	10.10 ± 0.09	110.6	3.5	E2
HD 26965	5147 ± 14	0.805 ± 0.004	4.52 ± 0.03	-0.24 ± 0.10	0.79 ± 0.05	10.04 ± 0.18	198.2	4.4	E2
HD 30652	6441 ± 19	1.322 ± 0.010	4.29 ± 0.02	0.00 ± 0.10	1.25 ± 0.05	9.28 ± 0.15	124.6	3.2	E2
HD 34411	5774 ± 44	1.331 ± 0.021	4.20 ± 0.03	0.05 ± 0.10	1.03 ± 0.04	9.92 ± 0.08	79.1	4.7	E2
HD 36395	3801 ± 9	0.574 ± 0.004	4.70 ± 0.01	0.35 ± 0.10	0.60 ± 0.01	9.76 ± 0.49	177.1	8.0	E1
HD 3651	5046 ± 86	0.947 ± 0.032	4.46 ± 0.04	0.15 ± 0.10	0.85 ± 0.04	10.12 ± 0.13	90.0	5.9	E2
HD 38858	5646 ± 45	0.933 ± 0.016	4.46 ± 0.04	-0.22 ± 0.10	0.91 ± 0.07	9.81 ± 0.28	65.6	6.0	E1
HD 39587	5898 ± 25	0.979 ± 0.009	4.47 ± 0.02	-0.04 ± 0.10	1.04 ± 0.04	9.27 ± 0.28	115.4	4.4	E2
HD 4628	4950 ± 14	0.695 ± 0.004	4.63 ± 0.02	-0.22 ± 0.10	0.75 ± 0.03	9.41 ± 0.44	134.0	5.7	E2
HD 48737	6478 ± 21	2.710 ± 0.021	3.80 ± 0.01	0.14 ± 0.10	1.70 ± 0.04	9.23 ± 0.03	57.0	3.4	E2
HD 49933	6635 ± 90	1.420 ± 0.040	4.21 ± 0.05	-0.39 ± 0.10	1.18 ± 0.09	9.49 ± 0.16	33.8	5.8	E1
HD 58946	6738 ± 55	1.655 ± 0.028	4.12 ± 0.03	-0.25 ± 0.10	1.32 ± 0.09	9.39 ± 0.11	54.1	4.2	E2
HD 6210	6089 ± 35	4.517 ± 0.152	3.37 ± 0.05	-0.01 ± 0.10	1.70 ± 0.15	9.21 ± 0.07	12.8	5.8	E1
HD 69897	6130 ± 58	1.387 ± 0.028	4.19 ± 0.04	-0.26 ± 0.10	1.07 ± 0.08	9.73 ± 0.12	55.2	5.1	E2
HD 75732	5172 ± 18	0.943 ± 0.010	4.43 ± 0.02	0.35 ± 0.10	0.88 ± 0.02	10.10 ± 0.09	79.8	6.0	E2
HD 79210	3907 ± 35	0.577 ± 0.013	4.70 ± 0.02	-0.18 ± 0.10	0.58 ± 0.02	9.85 ± 0.51	161.6	7.6	E2
HD 7924	5075 ± 83	0.782 ± 0.026	4.58 ± 0.04	-0.14 ± 0.10	0.81 ± 0.06	9.71 ± 0.52	58.8	7.2	E1
HD 82885	5376 ± 43	1.003 ± 0.016	4.40 ± 0.03	0.32 ± 0.10	0.92 ± 0.05	10.04 ± 0.15	89.5	5.3	E2
HD 86728	5619 ± 44	1.247 ± 0.021	4.24 ± 0.03	0.19 ± 0.10	0.98 ± 0.06	10.03 ± 0.11	67.1	5.4	E2
HD 88230	4085 ± 14	0.640 ± 0.005	4.64 ± 0.01	-0.16 ± 0.10	0.63 ± 0.01	10.14 ± 0.09	205.2	6.6	E2
HD 95735	3464 ± 15	0.392 ± 0.003	4.86 ± 0.01	-0.41 ± 0.10	0.40 ± 0.01	9.91 ± 0.47	392.4	7.5	E2
GJ 176	3679 ± 77	0.453 ± 0.022	4.80 ± 0.03	0.15 ± 0.10	0.49 ± 0.04	9.60 ± 0.53	106.3	10.0	E1
GL 144	5077 ± 35	0.735 ± 0.005	4.61 ± 0.02	-0.06 ± 0.10	0.80 ± 0.03	9.37 ± 0.39	310.8	3.7	E2
GL 338B	3867 ± 37	0.567 ± 0.014	4.71 ± 0.02	-0.15 ± 0.10	0.57 ± 0.02	9.82 ± 0.50	159.0	7.7	E1
GL 412A	3497 ± 39	0.398 ± 0.009	4.87 ± 0.02	-0.40 ± 0.10	0.41 ± 0.02	9.73 ± 0.52	206.9	8.8	E2

Table A1 continued

Table A1 (*continued*)

Name	T_{eff} K	R_{\star} R_{\odot}	$\log g$ dex	[Fe/H] dex	M_{\star} M_{\odot}	$\log_{10}(\text{age})$	π_{\star} mas	V mag	Notes
GL 570B	4507 ± 58	0.739 ± 0.019	4.60 ± 0.03	0.02 ± 0.10	0.73 ± 0.03	10.00 ± 0.48	133.6	5.7	E2
GL 687	3413 ± 28	0.418 ± 0.007	4.85 ± 0.01	-0.09 ± 0.10	0.43 ± 0.01	9.59 ± 0.52	220.0	9.2	E1
GL 699	3222 ± 10	0.187 ± 0.001	5.11 ± 0.01	-0.39 ± 0.10	0.16 ± 0.00	9.61 ± 0.54	549.0	9.5	E2
GL 702A	5407 ± 52	0.831 ± 0.004	4.56 ± 0.02	0.03 ± 0.10	0.92 ± 0.03	9.30 ± 0.35	—	4.1	E3
GL 702B	4393 ± 149	0.670 ± 0.009	4.64 ± 0.02	0.03 ± 0.10	0.71 ± 0.03	9.61 ± 0.52	—	7.2	E3
GL 876	3129 ± 19	0.376 ± 0.006	4.88 ± 0.01	0.19 ± 0.10	0.35 ± 0.01	10.09 ± 0.41	214.1	10.2	E1
HIP 57087	3416 ± 53	0.455 ± 0.018	4.83 ± 0.03	0.04 ± 0.10	0.45 ± 0.03	9.62 ± 0.52	102.6	10.6	E1
HIP 74995	3442 ± 54	0.299 ± 0.010	4.97 ± 0.03	-0.10 ± 0.10	0.30 ± 0.02	9.61 ± 0.53	158.6	10.6	E1
HIP 83043	3590 ± 45	0.539 ± 0.016	4.75 ± 0.02	-0.04 ± 0.10	0.52 ± 0.02	9.89 ± 0.48	96.4	9.7	E1

NOTE—Properties of stars in the `SpecMatch-Emp` library assembled from literature sources and this work.

^ABrewer et al. (2016) sample (§ 2.1.3). T_{eff} , $\log g$, [Fe/H] from single line fits to stellar models; M_{\star} , R_{\star} , age from isochrones.

^BAsteroseismic sample from Bruntt et al. (2012) (§ 2.1.4). $\log g$ from asteroseismic analysis; T_{eff} and [Fe/H] from individual spectral line fits; M_{\star} , R_{\star} and age from isochrones.

^CNew K-dwarf sample (§ 2.2). T_{eff} from empirical V-K color-temperature relationship; R_{\star} from combining T_{eff} with parallax and F_{bol} calculated from SED fitting; [Fe/H] from SME fitting in Gaidos et al. (2013); M_{\star} , $\log g$, age from isochrones.

^DMann et al. (2015) sample (§ 2.1.2). T_{eff} from stellar atmosphere models; R_{\star} from combining T_{eff} with F_{bol} obtained from flux-calibrated spectra; [Fe/H] and M_{\star} from empirical relationships; $\log g$ calculated directly from R_{\star} and M_{\star} ; age from isochrones.

^EInterferometric sample, as compiled in von Braun et al. (2014) (§ 2.1.1). R_{\star} from optical and infrared interferometry; T_{eff} and [Fe/H] by a variety of methods; M_{\star} , $\log g$ and age from isochrones.

¹Parallaxes from *Gaia* DR1 (Gaia Collaboration et al. 2016).

²Parallaxes from *Hipparcos* (van Leeuwen 2007).

³No parallaxes found.

REFERENCES

- Auvergne, M., Bodin, P., Boissard, L., et al. 2009, *A&A*, 506, 411
- Baines, E. K., McAlister, H. A., ten Brummelaar, T. A., et al. 2009, *ApJ*, 701, 154
- . 2008, *ApJ*, 680, 728
- Borucki, W. J., Koch, D., Basri, G., et al. 2010, *Science*, 327, 977
- Boyajian, T. S., von Braun, K., van Belle, G., et al. 2013, *ApJ*, 771, 40
- Brewer, J. M., Fischer, D. A., Basu, S., Valenti, J. A., & Piskunov, N. 2015, *ApJ*, 805, 126
- Brewer, J. M., Fischer, D. A., Valenti, J. A., & Piskunov, N. 2016, *ArXiv e-prints*, arXiv:1606.07929
- Bruntt, H., Basu, S., Smalley, B., et al. 2012, *MNRAS*, 423, 122
- Delfosse, X., Forveille, T., Ségransan, D., et al. 2000, *A&A*, 364, 217
- Dotter, A., Chaboyer, B., Jevremović, D., et al. 2008, *ApJS*, 178, 89
- Gaia Collaboration, Brown, A. G. A., Vallenari, A., et al. 2016, *ArXiv e-prints*, arXiv:1609.04172
- Gaidos, E., Fischer, D. A., Mann, A. W., & Howard, A. W. 2013, *ApJ*, 771, 18
- Gray, D. F. 1992, *The observation and analysis of stellar photospheres*.
- Gray, R. O., & Corbally, J., C. 2009, *Stellar Spectral Classification*
- Henry, G. W., Kane, S. R., Wang, S. X., et al. 2013, *ApJ*, 768, 155
- Howard, A. W., Johnson, J. A., Marcy, G. W., et al. 2010, *ApJ*, 721, 1467
- Huber, D., Chaplin, W. J., Christensen-Dalsgaard, J., et al. 2013, *ApJ*, 767, 127
- Kervella, P., Thévenin, F., Morel, P., Bordé, P., & Di Folco, E. 2003, *A&A*, 408, 681
- Kurucz, R. L., Furenlid, I., Brault, J., & Testerman, L. 1984, *Solar flux atlas from 296 to 1300 nm*
- Lindgren, L., Lammers, U., Bastian, U., et al. 2016, *ArXiv e-prints*, arXiv:1609.04303
- Mann, A. W., Brewer, J. M., Gaidos, E., Lépine, S., & Hilton, E. J. 2013, *AJ*, 145, 52
- Mann, A. W., Deacon, N. R., Gaidos, E., et al. 2014, *AJ*, 147, 160
- Mann, A. W., Feiden, G. A., Gaidos, E., Boyajian, T., & von Braun, K. 2015, *ApJ*, 804, 64
- Mann, A. W., & von Braun, K. 2015, *PASP*, 127, 102
- Michalik, D., Lindgren, L., & Hobbs, D. 2015, *A&A*, 574, A115
- Morgan, W. W., Keenan, P. C., & Kellman, E. 1943, *An atlas of stellar spectra, with an outline of spectral classification*
- Morton, T. D. 2015, *isochrones: Stellar model grid package, Astrophysics Source Code Library, , ascl:1503.010*

- Newville, M., Stensitzki, T., Allen, D. B., & Ingargiola, A. 2014, LMFIT: Non-Linear Least-Square Minimization and Curve-Fitting for Python, , doi:10.5281/zenodo.11813
- Perryman, M. A. C., Lindgren, L., Kovalevsky, J., et al. 1997, *A&A*, 323, L49
- Pickles, A. J. 1998, *PASP*, 110, 863
- Ricker, G. R., Winn, J. N., Vanderspek, R., et al. 2014, in *Proc. SPIE*, Vol. 9143, Space Telescopes and Instrumentation 2014: Optical, Infrared, and Millimeter Wave, 914320
- Snedden, C. A. 1973, PhD thesis, The University of Texas at Austin
- Torres, G., Andersen, J., & Giménez, A. 2010, *A&A Rv*, 18, 67
- Valenti, J. A., & Fischer, D. A. 2005, *ApJS*, 159, 141
- Valenti, J. A., & Piskunov, N. 1996, *A&AS*, 118, 595
- van Belle, G. T., & von Braun, K. 2009, *ApJ*, 694, 1085
- van Leeuwen, F. 2007, *A&A*, 474, 653
- Vogt, S. S., Allen, S. L., Bigelow, B. C., et al. 1994, in *Proc. SPIE*, Vol. 2198, Instrumentation in Astronomy VIII, ed. D. L. Crawford & E. R. Craine, 362
- von Braun, K., Boyajian, T. S., ten Brummelaar, T. A., et al. 2011a, *ApJ*, 740, 49
- von Braun, K., Boyajian, T. S., Kane, S. R., et al. 2011b, *ApJL*, 729, L26
- . 2012, *ApJ*, 753, 171
- von Braun, K., Boyajian, T. S., van Belle, G. T., et al. 2014, *MNRAS*, 438, 2413